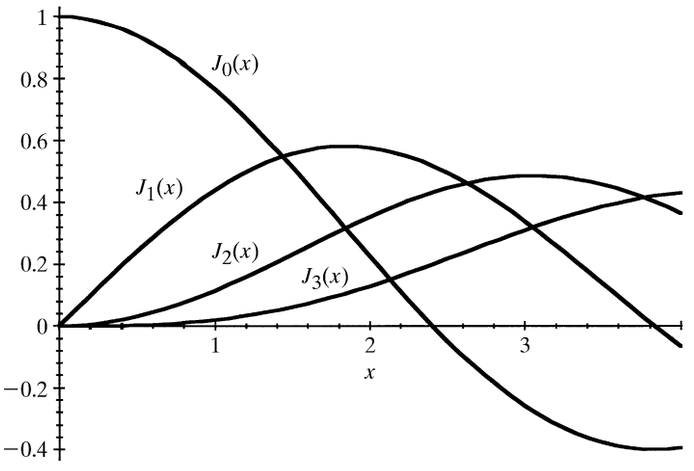

Fig. 4.6.3.4. The relative structure-factor magnitudes of mth-order satellite reflections for a harmonic displacive modulation are proportional to the values of the mth-order Bessel function $J_m(x)$.

$i = 1, \ldots, 3$. In the general case, each subsystem will be modulated with the periods of the others due to their mutual interactions. Thus, in general, CSs consist of several intergrown incommensurately modulated substructures. The satellite vectors $\mathbf{q}_{j\nu}$, $j = 1, \ldots, d$, referred to the νth subsystem can be obtained from M^* by applying the $d \times (3+d)$ integer matrices $V_{jk\nu}$: $\mathbf{q}_{j\nu} = \sum_{k=1}^{3+d} V_{jk\nu}\mathbf{a}_k^*$, $j = 1, \ldots, d$. The matrices consisting of the components σ_ν of the satellite vectors $\mathbf{q}_{j\nu}$ with regard to the reciprocal sublattices Λ_ν^* can be calculated by $\sigma_\nu = (V_{3\nu} + V_{d\nu}\sigma)(Z_{3\nu} + Z_{d\nu}\sigma)^{-1}$, where the subscript 3 refers to the 3×3 submatrix of physical space and the subscript d to the $d \times d$ matrix of the internal space. The juxtaposition of the $3 \times (3+d)$ matrix Z_ν and the $d \times (3+d)$ matrix V_ν defines the non-singular $(3+d) \times (3+d)$ matrix W_ν,

$$W_\nu = \begin{pmatrix} Z_\nu \\ V_\nu \end{pmatrix}.$$

This matrix allows the reinterpretation of the Fourier module M^* as the Fourier module $M_\nu^* = M^* W_\nu$ of a d-dimensionally modulated subsystem ν. It also describes the coordinate transformation between the superspace basis Σ and Σ_ν.

The superspace description is obtained analogously to that for IMSs (see Section 4.6.3.1) by considering the 3D Fourier module M^* of rank $3+d$ as the projection of a $(3+d)$D reciprocal lattice Σ^* upon the physical space. Thus, one obtains for the definition of the direct and reciprocal $(3+d)$ lattices (Janner & Janssen, 1980*b*)

$$\Sigma^* : \begin{cases} \mathbf{a}_i^* & = (\mathbf{a}_i^*, \mathbf{0}) & i = 1, \ldots, 3 \\ \mathbf{a}_{3+j}^* & = (\mathbf{a}_{3+j}^*, \mathbf{e}_j^*) & j = 1, \ldots, d \end{cases}$$

$$\Sigma : \begin{cases} \mathbf{a}_i & = (\mathbf{a}_i, -\sum_{j=1}^{d} \sigma_{ji}\mathbf{e}_j) & i = 1, \ldots, 3 \\ \mathbf{a}_{3+j} & = (\mathbf{0}, \mathbf{e}_j) & j = 1, \ldots, d. \end{cases}$$

4.6.3.2.1. *Indexing*

The indexing of diffraction patterns of composite structures can be performed in the following way:

(1) find the minimum number of reciprocal lattices Λ_ν^* necessary to index the diffraction pattern;

(2) find a basis for M^*, the union of sublattices Λ_ν^*;

(3) find the appropriate superspace embedding.

The $(3+d)$ vectors $\mathbf{a}_i^*$ forming a basis for the 3D Fourier module $M^* = \{\sum_{i=1}^{3+d} h_i \mathbf{a}_i^*\}$ can be chosen such that $\mathbf{a}_1^*$, $\mathbf{a}_2^*$ and $\mathbf{a}_3^*$ are linearly independent. Then the remaining d vectors can be described as a linear combination of the first three, defining the $d \times 3$ matrix σ: $\mathbf{a}_{3+j}^* = \sum_{i=1}^{3+d} \sigma_{ji}\mathbf{a}_i^*$, $j = 1, \ldots, d$. This is formally equivalent to the reciprocal basis obtained for an IMS (see Section 4.6.3.1) and one can proceed in an analogous way to that for IMSs.

4.6.3.2.2. *Diffraction symmetry*

The symmetry of CSs can be described with basically the same formalism as used for IMSs. This is a consequence of the formally equivalent applicability of the higher-dimensional approach, in particular of the superspace-group theory developed for IMSs [see Janner & Janssen (1980*a*,*b*); van Smaalen (1991, 1992); Yamamoto (1992*a*)].

4.6.3.2.3. *Structure factor*

The structure factor $F(\mathbf{H})$ of a composite structure consists of the weighted contributions of the subsystem structure factors $F_\nu(\mathbf{H}_\nu)$:

$$F(\mathbf{H}) = \sum_\nu |J_\nu| F_\nu(\mathbf{H}_\nu);$$

$$F_\nu(\mathbf{H}) = \sum_{(R^\nu, \mathbf{t}^\nu)}^{\infty} \sum_{k=1}^{N'} \int_0^1 \mathrm{d}\bar{x}_{4,k}^\nu \ldots \int_0^1 \mathrm{d}\bar{x}_{3+d,k}^\nu f_k^\nu(\mathbf{H}^\parallel) p_k^\nu \times \exp\left(-\sum_{i,j=1}^{3+d} h_i^\nu [R^\nu B_{ijk}^\nu R^{\nu T}] h_j^\nu + 2\pi i \sum_{j=1}^{3+d} h_j^\nu R^\nu x_{jk}^\nu + h_j^\nu t_j^\nu \right),$$

with coefficients similar to those for IMSs.

The weights are the Jacobians of the transformations from $\mathbf{t}_\nu$ to $\mathbf{t}$, and $\mathbf{H}_\nu$ are the reflection indices with respect to the subsystem Fourier modules M_ν^* (van Smaalen, 1995, and references therein). The relative values of $|J_\nu|$, where $J_\nu = \det\left[(V_{d\nu} - \sigma_\nu \cdot Z_{d\nu})^{-1}\right]$, are related to the volume ratios of the contributing subsystems. The subsystem structure factors correspond to those for IMSs (see Section 4.6.3.1). Besides this formula, based on the publications of Yamamoto (1982) and van Smaalen (1995), different structure-factor equations have been discussed (Kato, 1990; Petricek, Maly, Coppens *et al.*, 1991).

4.6.3.3. *Quasiperiodic structures (QSs)*

4.6.3.3.1. *3D structures with 1D quasiperiodic order*

Structures with quasiperiodic order in one dimension and lattice symmetry in the other two dimensions are the simplest representatives of quasicrystals. A few phases of this structure type have been identified experimentally (*see* Steurer, 1990). Since the Fibonacci chain represents the most important model of a 1D quasiperiodic structure, it will be used in this section to represent the quasiperiodic direction of 3D structures with 1D quasiperiodic order. As discussed in Section 4.6.2.4, 1D quasiperiodic structures are on the borderline between quasiperiodic and incommensurately modulated structures. They can be described using either of the two approaches. In the following, the quasiperiodic description will be preferred to take account of the scaling symmetry.

The electron-density-distribution function $\rho(\mathbf{r})$ of a 1D quasiperiodically ordered 3D crystal can be represented by a Fourier series:

$$\rho(\mathbf{r}) = (1/V) \sum_{\mathbf{H}} F(\mathbf{H}) \exp(-2\pi_i \mathbf{H} \cdot \mathbf{r}).$$

The Fourier coefficients (*structure factors*) $F(\mathbf{H})$ differ from zero only for reciprocal-space vectors $\mathbf{H} = \sum_{i=1}^{3} h_i^\parallel \mathbf{a}_i^*$ with $h_1{}^\parallel \in \mathbb{R}$, $h_2{}^\parallel, h_3{}^\parallel \in \mathbb{Z}$ or with integer indexing $\mathbf{H} = \sum_{i=1}^{4} h_i \mathbf{a}_i^*$ with $h_i \in \mathbb{Z}$. The set of all vectors $\mathbf{H}$ forms a Fourier module $M^* = \{\mathbf{H}^\parallel = \sum_{i=1}^{4} h_i \mathbf{a}_i^* | h_i \in \mathbb{Z}\}$ of rank 4 which can be decomposed into two rank 2 submodules $M^* = M_1^* \oplus M_2^*$. $M_1^* = \{h_1 \mathbf{a}_1^* + h_2 \mathbf{a}_2^*\}$ corresponds

to a $\mathbb{Z}$ module of rank 2 in a 1D subspace, $M_2^* = \{h_3\mathbf{a}_3^* + h_4\mathbf{a}_4^*\}$ corresponds to a $\mathbb{Z}$ module of rank 2 in a 2D subspace. Consequently, the first submodule can be considered as a projection from a 2D reciprocal lattice, $M_1^* = \pi^{\parallel}(\Sigma^*)$, while the second submodule is of the form of a reciprocal lattice, $M_2^* = \Lambda^*$.

Hence, the reciprocal-basis vectors $\mathbf{a}_i^*$, $i = 1, \ldots, 4$, can be considered to be projections of reciprocal-basis vectors $\mathbf{d}_i^*, i = 1, \ldots, 4$, spanning a 4D reciprocal lattice, onto the physical space $\Sigma^* = \{\mathbf{H} = \sum_{i=1}^4 h_i\mathbf{d}_i^* | h_i \in \mathbb{Z}\}$, with

$$\mathbf{d}_1^* = a_1^*\begin{pmatrix}1\\-\tau\\0\\0\end{pmatrix},\ \mathbf{d}_2^* = a_1^*\begin{pmatrix}\tau\\1\\0\\0\end{pmatrix},\ \mathbf{d}_3^* = a_3^*\begin{pmatrix}0\\0\\1\\0\end{pmatrix},\ \mathbf{d}_4^* = a_4^*\begin{pmatrix}0\\0\\0\\1\end{pmatrix}.$$

A direct lattice Σ with basis $\mathbf{d}_i, i = 1, \ldots, 4$ and $\mathbf{d}_i \cdot \mathbf{d}_j^* = \delta_{ij}$, can be constructed according to (compare Fig. 4.6.2.8) $\Sigma = \{\mathbf{r} = \sum_{i=1}^4 m_i\mathbf{d}_i | m_i \in \mathbb{Z}\}$, with

$$\mathbf{d}_1 = \frac{1}{a_1^*(2+\tau)}\begin{pmatrix}1\\-\tau\\0\\0\end{pmatrix}, \mathbf{d}_2 = \frac{1}{a_1^*(2+\tau)}\begin{pmatrix}\tau\\1\\0\\0\end{pmatrix},$$

$$\mathbf{d}_3^* = \frac{1}{a_3^*}\begin{pmatrix}0\\0\\1\\0\end{pmatrix},\ \mathbf{d}_4^* = \frac{1}{a_4^*}\begin{pmatrix}0\\0\\0\\1\end{pmatrix}.$$

Consequently, the structure in physical space $\mathbf{V}^{\parallel}$ is equivalent to a 3D section of the 4D hypercrystal.

4.6.3.3.1.1. *Indexing*

The reciprocal space of the Fibonacci chain is densely filled with Bragg reflections (Figs. 4.6.2.9 and 4.6.3.5). According to the nD embedding method, the shorter the parallel-space distance $\Delta\mathbf{H}^{\parallel} = \mathbf{H}_2^{\parallel} - \mathbf{H}_1^{\parallel}$ between two Bragg reflections, the larger the corresponding perpendicular-space distance $\Delta\mathbf{H}^{\perp} = \mathbf{H}_2^{\perp} - \mathbf{H}_1^{\perp}$ becomes. Since the structure factor $F(\mathbf{H})$ decreases rapidly as a function of $\mathbf{H}^{\perp}$ (Fig. 4.6.3.6), 'neighbouring' reflections of strong Bragg peaks are extremely weak and, consequently, the reciprocal space appears to be filled with *discrete* Bragg peaks even for low-resolution experiments.

This property allows an unambiguous identification of a correct set of reciprocal-basis vectors. However, infinitely many sets allowing a correct indexing of the diffraction pattern with integer indices exist. Nevertheless, an optimum basis (low indices are assigned to strong reflections) can be derived: the intensity distribution, not the metrics, characterizes the best choice of indexing. Once the minimum distance S in the structure is identified from chemical considerations, the reciprocal basis should be chosen as described in Section 4.6.2.4. It has to be kept in mind, however, that the identification of the metrics is not sufficient to distinguish in the 1D aperiodic case between an incommensurately modulated structure, a quasiperiodic structure or special kinds of structures with fractally shaped atomic surfaces.

A correct set of reciprocal-basis vectors can be identified in the following way:

(1) Find pairs of strong reflections whose physical-space diffraction vectors are related to each other by the factor τ.

(2) Index these reflections by assigning an appropriate value to a^*. This value should be derived from the shortest interatomic distance S expected in the structure.

(3) The reciprocal basis is correct if all observable Bragg reflections can be indexed with integer numbers.

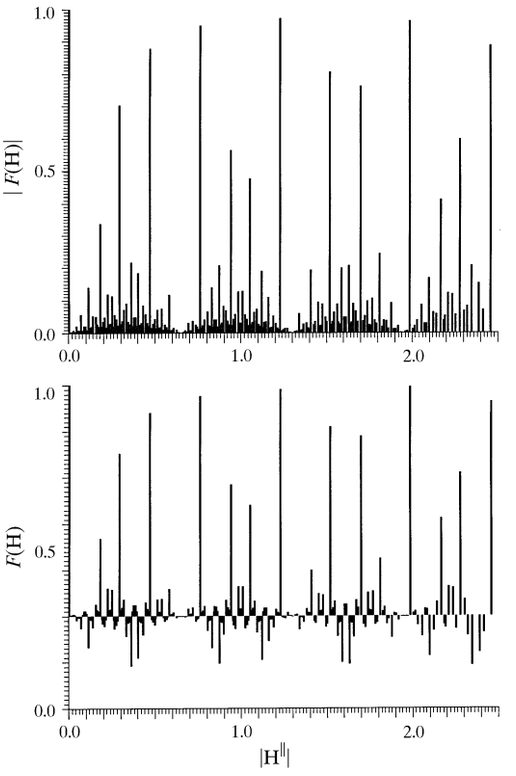

Fig. 4.6.3.5. The structure factors $F(\mathbf{H})$ (below) and their magnitudes $|F(\mathbf{H})|$ (above) of a Fibonacci chain decorated with equal point atoms are shown as a function of the parallel-space component $|\mathbf{H}^{\parallel}|$ of the diffraction vector. The short distance in the Fibonacci chain is S = 2.5 Å, all structure factors within $0 \le |\mathbf{H}| \le 2.5$ Å^{-1} have been calculated and normalized to $F(00) = 1$.

4.6.3.3.1.2. *Diffraction symmetry*

The possible Laue symmetry group K^{3D} of the Fourier module $M^* = \{\mathbf{H}^{\parallel} = \sum_{i=1}^4 h_i\mathbf{a}_i^* | h_i \in \mathbb{Z}\}$ is any one of the direct product $K^{3D} = K^{2D} \otimes K^{1D} \otimes \bar{1}$. K^{2D} corresponds to one of the ten crystallographic 2D point groups, $K^{1D} = \{1\}$ in the general case of a quasiperiodic stacking of periodic layers. Consequently, the nine Laue groups $\bar{1}$, $2/m$, mmm, $4/m$, $4/mmm$, $\bar{3}$, $\bar{3}m$, $6/m$ and $6/mmm$ are possible. These are all 3D crystallographic Laue groups except for the two cubic ones.

The (unweighted) Fourier module shows only 2D lattice symmetry. In the third dimension, the submodule M_1^* remains invariant under the scaling symmetry operation $S^nM_1^* = \tau^nM_1^*$ with $n \in \mathbb{Z}$. The scaling symmetry operators S^n form an infinite group $s = \{\ldots, S^{-1}, S^0, S^1, \ldots\}$ of reciprocal-basis transformations S^n in superspace,

$$S^n = \begin{pmatrix}0&1&0&0\\1&1&0&0\\0&0&1&0\\0&0&0&1\end{pmatrix}_D^n,\ S^{-1} = \begin{pmatrix}\bar{1}&1&0&0\\1&0&0&0\\0&0&1&0\\0&0&0&1\end{pmatrix}_D,$$

$$S^0 = \begin{pmatrix}1&0&0&0\\0&1&0&0\\0&0&1&0\\0&0&0&1\end{pmatrix}_D,$$

and act on the reciprocal basis $\mathbf{d}_i^*$ in superspace.

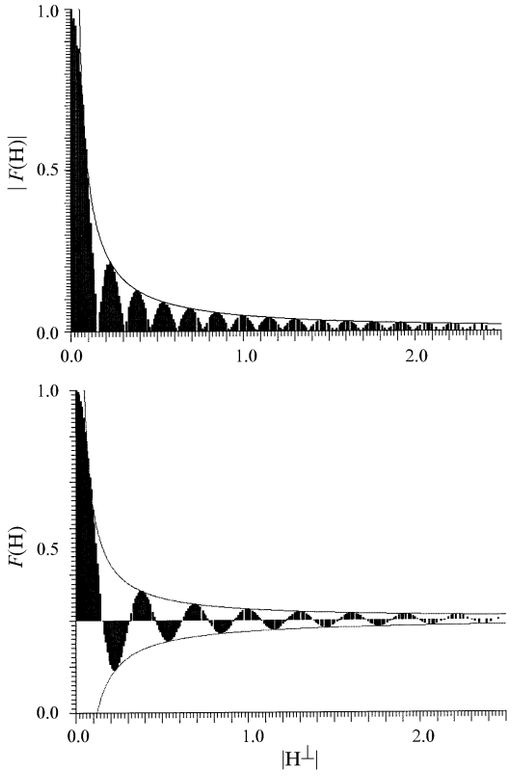

Fig. 4.6.3.6. The structure factors $F(\mathbf{H})$ (below) and their magnitudes $|F(\mathbf{H})|$ (above) of a Fibonacci chain decorated with equal point atoms are shown as a function of the perpendicular-space component $|\mathbf{H}^{\perp}|$ of the diffraction vector. The short distance in the Fibonacci chain is S = 2.5 Å, all structure factors within $0 \leq |\mathbf{H}| \leq 2.5$ Å^{-1} have been calculated and normalized to $F(00) = 1$.

4.6.3.3.1.3. *Structure factor*

The structure factor of a periodic structure is defined as the Fourier transform of the density distribution $\rho(\mathbf{r})$ of its unit cell (UC):

$$F(\mathbf{H}) = \int_{\mathrm{UC}} \rho(\mathbf{r}) \exp(2\pi i \mathbf{H} \cdot \mathbf{r})\, \mathrm{d}\mathbf{r}.$$

The same is valid in the case of the nD description of a quasiperiodic structure. The parallel- and perpendicular-space components are orthogonal to each other and can be separated. In the case of the 1D Fibonacci sequence, the Fourier transform of the parallel-space component of the electron-density distribution of a single atom gives the usual atomic scattering factor $f(\mathbf{H}^{\parallel})$. Parallel to $x^{\perp}$, $\rho(\mathbf{r})$ adopts values $\neq 0$ only within the interval $-(1+\tau)/[2a^*(2+\tau)] \leq x^{\perp} \leq (1+\tau)/[2a^*(2+\tau)]$ and one obtains

$$F(\mathbf{H}) = f(\mathbf{H}^{\parallel})[a^*(2+\tau)]/(1+\tau) \times \int_{-(1+\tau)/[2a^*(2+\tau)]}^{+(1+\tau)/[2a^*(2+\tau)]} \exp(2\pi i \mathbf{H}^{\perp} \cdot x^{\perp})\, \mathrm{d}x^{\perp}.$$

The factor $[a^*(2+\tau)]/(1+\tau)$ results from the normalization of the structure factors to $F(\mathbf{0}) = f(0)$. With

$$\mathbf{H} = h_1\mathbf{d}_1^* + h_2\mathbf{d}_2^* + h_3\mathbf{d}_3^* + h_4\mathbf{d}_4^* = h_1 a_1^* \begin{pmatrix} 1 \\ -\tau \\ 0 \\ 0 \end{pmatrix} + h_2 a_1^* \begin{pmatrix} \tau \\ 1 \\ 0 \\ 0 \end{pmatrix} + h_3 a_3^* \begin{pmatrix} 0 \\ 0 \\ 1 \\ 0 \end{pmatrix} + h_4 a_4^* \begin{pmatrix} 0 \\ 0 \\ 0 \\ 1 \end{pmatrix}$$

and $\mathbf{H}^{\perp} = a_1^*(-\tau h_1 + h_2)$ the integrand can be rewritten as

$$F(\mathbf{H}) = f(\mathbf{H}^{\parallel})[a^*(2+\tau)]/(1+\tau) \times \int_{-(1+\tau)/[2a^*(2+\tau)]}^{+(1+\tau)/[2a^*(2+\tau)]} \exp[2\pi i(-\tau h_1 + h_2)x^{\perp}]\, \mathrm{d}x^{\perp},$$

yielding

$$F(\mathbf{H}) = f(\mathbf{H}^{\parallel})(2+\tau)/[2\pi i(-\tau h_1 + h_2)(1+\tau)] \times \exp[2\pi i(-\tau h_1 + h_2)x^{\perp}]\Big|_{-(1+\tau)/[2a^*(2+\tau)]}^{+(1+\tau)/[2a^*(2+\tau)]}.$$

Using $\sin x = (\mathrm{e}^{ix} - \mathrm{e}^{-ix})/2i$ gives

$$F(\mathbf{H}) = f(\mathbf{H}^{\parallel})(2+\tau)/[\pi(-\tau h_1 + h_2)(1+\tau)] \times \sin[\pi(1+\tau)(-\tau h_1 + h_2)]/(2+\tau).$$

Thus, the structure factor has the form of the function $\sin(x)/x$ with x a perpendicular reciprocal-space coordinate. The upper and lower limiting curves of this function are given by the hyperbolae $\pm 1/x$ (Fig. 4.6.3.6). The continuous shape of $F(\mathbf{H})$ as a function of $\mathbf{H}^{\perp}$ allows the estimation of an overall temperature factor and atomic scattering factor for reflection-data normalization (compare Figs. 4.6.3.6 and 4.6.3.7).

In the case of a 3D crystal structure which is quasiperiodic in one direction, the structure factor can be written in the form

$$F(\mathbf{H}) = \sum_{k=1}^{n} \Big[T_k(\mathbf{H}) f_k(\mathbf{H}^{\parallel}) g_k(\mathbf{H}^{\perp}) \exp(2\pi i \mathbf{H} \cdot \mathbf{r}_k) \Big].$$

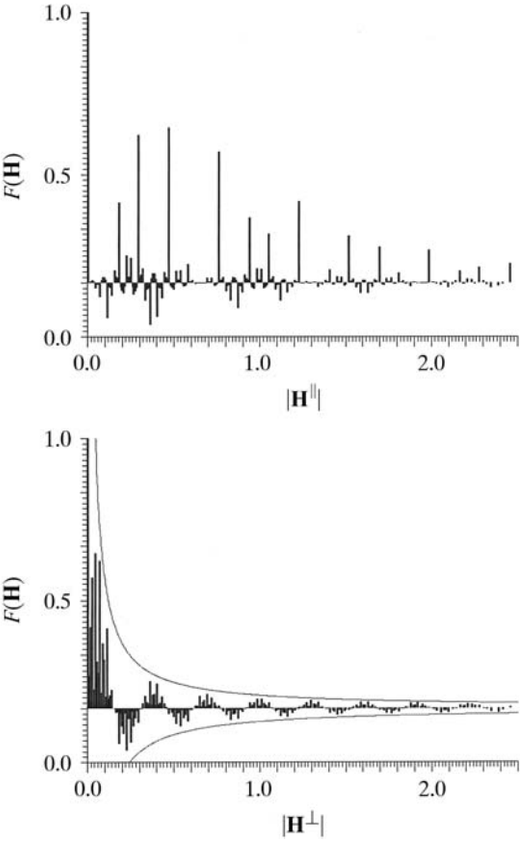

Fig. 4.6.3.7. The structure factors $F(\mathbf{H})$ of the Fibonacci chain decorated with aluminium atoms ($U_{\mathrm{overall}} = 0.005$ Å^2) as a function of the parallel (above) and the perpendicular (below) component of the diffraction vector. The short distance is S = 2.5 Å, all structure factors within $0 \leq |\mathbf{H}| \leq 2.5$ Å^{-1} have been calculated and normalized to $F(00) = 1$.

The sum runs over all n averaged hyperatoms in the 4D unit cell of the structure. The *geometric form factor* $g_k(\mathbf{H}^\perp)$ corresponds to the Fourier transform of the kth atomic surface,

$$g_k(\mathbf{H}^\perp) = (1/A^\perp_{\rm UC}) \int_{A_k} \exp(2\pi i \mathbf{H}^\perp \cdot \mathbf{r}^\perp)\ \mathrm{d}\mathbf{r}^\perp,$$

normalized to $A^\perp_{\rm UC}$, the area of the 2D unit cell projected upon $\mathbf{V}^\perp$, and A_k, the area of the kth atomic surface.

The atomic temperature factor $T_k(\mathbf{H})$ can also have perpendicular-space components. Assuming only harmonic (static or dynamic) displacements in parallel and perpendicular space one obtains, in analogy to the usual expression (Willis & Pryor, 1975),

$$\begin{aligned} T_k(\mathbf{H}) &= T_k(\mathbf{H}^\parallel, \mathbf{H}^\perp) \\ &= \exp(-2\pi^2 \mathbf{H}^{\parallel T} \langle \mathbf{u}_i^\parallel \mathbf{u}_j^{\parallel T} \rangle \mathbf{H}^\parallel) \exp(-2\pi^2 \mathbf{H}^{\perp T} \langle \mathbf{u}_i^\perp \mathbf{u}_j^{\perp T} \rangle \mathbf{H}^\perp), \end{aligned}$$

with

$$\langle \mathbf{u}_i^\parallel \mathbf{u}_j^{\parallel T} \rangle = \begin{pmatrix} \langle \mathbf{u}_1^{\parallel 2} \rangle & \langle \mathbf{u}_1^\parallel \cdot \mathbf{u}_2^{\parallel T} \rangle & \langle \mathbf{u}_1^\parallel \cdot \mathbf{u}_3^{\parallel T} \rangle \\ \langle \mathbf{u}_2^\parallel \cdot \mathbf{u}_1^{\parallel T} \rangle & \langle \mathbf{u}_2^{\parallel 2} \rangle & \langle \mathbf{u}_2^\parallel \cdot \mathbf{u}_3^{\parallel T} \rangle \\ \langle \mathbf{u}_3^\parallel \cdot \mathbf{u}_1^{\parallel T} \rangle & \langle \mathbf{u}_3^\parallel \cdot \mathbf{u}_2^{\parallel T} \rangle & \langle \mathbf{u}_3^{\parallel 2} \rangle \end{pmatrix}$$

$$\text{and } \langle \mathbf{u}_i^\perp \mathbf{u}_j^{\perp T} \rangle = \langle \mathbf{u}_4^\perp \rangle.$$

The elements of the type $\langle \mathbf{u}_i \cdot \mathbf{u}_j^T \rangle$ represent the average values of the atomic displacements along the ith axis times the displacement along the jth axis on the V basis.

4.6.3.3.1.4. *Intensity statistics*

In the following, only the properties of the quasiperiodic component of the 3D structure, namely the Fourier module M_1^*, are discussed. The intensities $I(\mathbf{H})$ of the Fibonacci chain decorated with point atoms are only a function of the perpendicular-space component of the diffraction vector. $|F(\mathbf{H})|$ and $F(\mathbf{H})$ are illustrated in Figs. 4.6.3.5 and 4.6.3.6 as a function of $\mathbf{H}^\parallel$ and of $\mathbf{H}^\perp$. The distribution of $|F(\mathbf{H})|$ as a function of their frequencies clearly resembles a centric distribution, as can be expected from the centrosymmetric 2D sub-unit cell. The shape of the distribution function depends on the radius $H_{\rm max}$ of the limiting sphere in reciprocal space. The number of weak reflections increases with the square of $H_{\rm max}$, that of strong reflections only linearly (strong reflections always have small $\mathbf{H}^\perp$ components).

The weighted reciprocal space of the Fibonacci sequence contains an infinite number of Bragg reflections within a limited region of the physical space. Contrary to the diffraction pattern of a periodic structure consisting of point atoms on the lattice nodes, the Bragg reflections show intensities depending on the perpendicular-space components of their diffraction vectors.

The reciprocal space of a sequence generated from hyperatoms with fractally shaped atomic surfaces (squared Fibonacci sequence) is very similar to that of the Fibonacci sequence (Figs. 4.6.3.8 and 4.6.3.9). However, there are significantly more weak reflections in the diffraction pattern of the 'fractal' sequence, caused by the geometric form factor.

4.6.3.3.1.5. *Relationships between structure factors at symmetry-related points of the Fourier image*

The two possible point-symmetry groups in the 1D quasiperiodic case, $K^{\rm 1D} = 1$ and $K^{\rm 1D} = \bar{1}$, relate the structure factors to

$$\begin{aligned} 1 &: \quad F(\mathbf{H}) = -F(\bar{\mathbf{H}}), \\ \bar{1} &: \quad F(\mathbf{H}) = F(\bar{\mathbf{H}}). \end{aligned}$$

A 3D structure with 1D quasiperiodicity results from the stacking of atomic layers with distances following a quasiperiodic sequence.

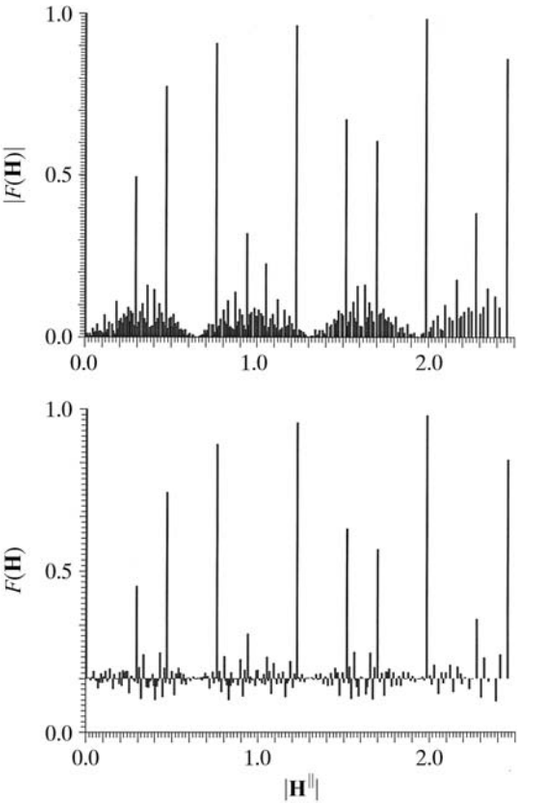

Fig. 4.6.3.8. The structure factors $F(\mathbf{H})$ (below) and their magnitudes $|F(\mathbf{H})|$ (above) of the squared Fibonacci chain decorated with equal point atoms are shown as a function of the parallel-space component $|\mathbf{H}^\parallel|$ of the diffraction vector. The short distance is $\mathrm{S} = 2.5$ Å^{-1}, all structure factors within $0 \le |\mathbf{H}| \le 2.5$ Å^{-1} have been calculated and normalized to $F(00) = 1$.

The point groups $K^{\rm 3D}$ describing the symmetry of such structures result from the direct product $K^{\rm 3D} = K^{\rm 2D} \otimes K^{\rm 1D}$. $K^{\rm 2D}$ corresponds to one of the ten crystallographic 2D point groups, $K^{\rm 1D}$ can be $\{1\}$ or $\{1, m\}$. Consequently, 18 3D point groups are possible.

Since 1D quasiperiodic sequences can be described generically as incommensurately modulated structures, their possible point and space groups are equivalent to a subset of the $(3+1)$D superspace groups for IMSs with satellite vectors of the type (00γ), *i.e.* $\mathbf{q} = \gamma \mathbf{c}^*$, for the quasiperiodic direction [001] (Janssen *et al.*, 1999).

From the scaling properties of the Fibonacci sequence, some relationships between structure factors can be derived. Scaling the physical-space structure by a factor τ^n, $n \in \mathbb{Z}$, corresponds to a scaling of the perpendicular space by the inverse factor $(-\tau)^{-n}$. For the scaling of the corresponding reciprocal subspaces, the inverse factors compared to the direct spaces have to be applied.

The set of vectors $\mathbf{r}$, defining the vertices of a Fibonacci sequence $s(\mathbf{r})$, multiplied by a factor τ coincides with a subset of the vectors defining the vertices of the original sequence (Fig. 4.6.3.10). The residual vertices correspond to a particular decoration of the scaled sequence, *i.e.* the sequence $\tau^2 s(\mathbf{r})$. The Fourier transform of the sequence $s(\mathbf{r})$ then can be written as the sum of the Fourier transforms of the sequences $\tau s(\mathbf{r})$ and $\tau^2 s(\mathbf{r})$;

$$\sum_k \exp(2\pi i \mathbf{H} \cdot \mathbf{r}_k) = \sum_k \exp(2\pi i \mathbf{H} \tau \mathbf{r}_k) + \sum_k \exp[2\pi i \mathbf{H}(\tau^2 \mathbf{r}_k + \tau)].$$

In terms of structure factors, this can be reformulated as

$$F(\mathbf{H}) = F(\tau \mathbf{H}) + \exp(2\pi i \tau \mathbf{H}) F(\tau^2 \mathbf{H}).$$

Hence, phases of structure factors that are related by scaling symmetry can be determined from each other.

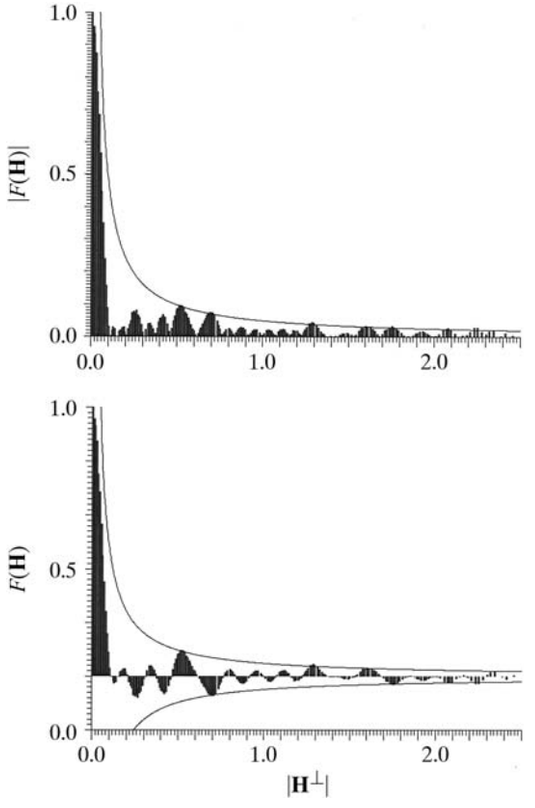

Fig. 4.6.3.9. The structure factors $F(\mathbf{H})$ (below) and their magnitudes $|F(\mathbf{H})|$ (above) of the squared Fibonacci chain decorated with equal point atoms are shown as a function of the perpendicular-space component $|\mathbf{H}^{\perp}|$ of the diffraction vector. The short distance is S = 2.5 Å, all structure factors within $0 \le |\mathbf{H}| \le 2.5$ Å^{-1} have been calculated and normalized to $F(00) = 1$.

Further scaling relationships in reciprocal space exist: scaling a diffraction vector $\mathbf{H} = h_1\mathbf{d}_1^* + h_2\mathbf{d}_2^* = h_1 a^* \begin{pmatrix} 1 \\ -\tau \end{pmatrix}_V + h_2 a^* \begin{pmatrix} \tau \\ 1 \end{pmatrix}_V$ with the matrix $S = \begin{pmatrix} 0 & 1 \\ 1 & 1 \end{pmatrix}_D$,

$$\begin{pmatrix} 0 & 1 \\ 1 & 1 \end{pmatrix}_D \begin{pmatrix} h_1 \\ h_2 \end{pmatrix}_D = \begin{pmatrix} F_n & F_{n+1} \\ F_{n+1} & F_{n+2} \end{pmatrix}_D \begin{pmatrix} h_1 \\ h_2 \end{pmatrix}_D = \begin{pmatrix} F_n h_1 + F_{n+1} h_2 \\ F_{n+1} h_1 + F_{n+2} h_2 \end{pmatrix}_D,$$

increases the magnitudes of structure factors assigned to this particular diffraction vector $\mathbf{H}$,

$$\left|F(S^n\mathbf{H})\right| > \left|F(S^{n-1}\mathbf{H})\right| > \ldots > \left|F(S\mathbf{H})\right| > \left|F(\mathbf{H})\right|.$$

This is due to the shrinking of the perpendicular-space component of the diffraction vector by powers of $(-\tau)^{-n}$ while expanding the parallel-space component by τ^n according to the eigenvalues τ and $-\tau^{-1}$ of S acting in the two eigenspaces $\mathbf{V}^{\parallel}$ and $\mathbf{V}^{\perp}$:

$$\begin{aligned} \pi^{\parallel}(S\mathbf{H}) &= (h_2 + \tau(h_1 + h_2))a^* = (\tau h_1 + h_2(\tau + 1))a^* \\ &= \tau(h_1 + \tau h_2)a^*, \\ \pi^{\perp}(S\mathbf{H}) &= (-\tau h_2 + h_1 + h_2)a^* = (h_1 - h_2(\tau - 1))a^* \\ &= -(1/\tau)(-\tau h_1 + h_2)a^*, \\ \left|F(\tau^n\mathbf{H}^{\parallel})\right| &> \left|F(\tau^{n-1}\mathbf{H}^{\parallel})\right| > \ldots > \left|F(\tau\mathbf{H}^{\parallel})\right| > \left|F(\mathbf{H}^{\parallel})\right|. \end{aligned}$$

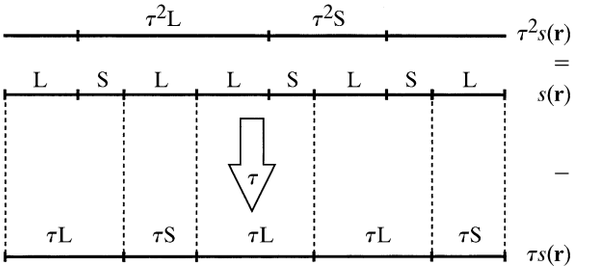

Fig. 4.6.3.10. Part . . . LSLLSLSL . . . of a Fibonacci sequence $s(\mathbf{r})$ before and after scaling by the factor τ. L is mapped onto τL, S onto τS = L. The vertices of the new sequence are a subset of those of the original sequence (the correspondence is indicated by dashed lines). The residual vertices $\tau^2 s(\mathbf{r})$, which give when decorating $\tau s(\mathbf{r})$ the Fibonacci sequence $s(\mathbf{r})$, form a Fibonacci sequence scaled by a factor τ^2.

Thus, for scaling n times we obtain

$$\begin{aligned} \pi^{\perp}(S^n\mathbf{H}) &= (-\tau(F_n h_1 + F_{n+1} h_2) + (F_{n+1} h_1 + F_{n+2} h_2))a^* \\ &= (h_1(-\tau F_n + F_{n+1}) + h_2(-\tau F_{n+1} + F_{n+2}))a^* \end{aligned}$$

with

$$\lim_{n\to\infty}(-\tau F_n + F_{n+1}) = 0 \text{ and } \lim_{n\to\infty}(-\tau F_{n+1} + F_{n+2}) = 0,$$

yielding eventually

$$\lim_{n\to\infty}\left(\pi^{\perp}(S^n\mathbf{H})\right) = 0 \text{ and } \lim_{n\to\infty}(F(S^n\mathbf{H})) = F(\mathbf{0}).$$

The scaling of the diffraction vectors $\mathbf{H}$ by S^n corresponds to a hyperbolic rotation (Janner, 1992) with angle $n\varphi$, where $\sinh\varphi = 1/2$ (Fig. 4.6.3.11):

$$\begin{pmatrix} 0 & 1 \\ 1 & 1 \end{pmatrix}^{2n} = \begin{pmatrix} \cosh 2n\varphi & \sinh 2n\varphi \\ \sinh 2n\varphi & \cosh 2n\varphi \end{pmatrix},$$

$$\begin{pmatrix} 0 & 1 \\ 1 & 1 \end{pmatrix}^{2n+1} = \begin{pmatrix} \sinh[(2n+1)\varphi] & \cosh[(2n+1)\varphi] \\ \cosh[(2n+1)\varphi] & \sinh[(2n+1)\varphi] \end{pmatrix}.$$

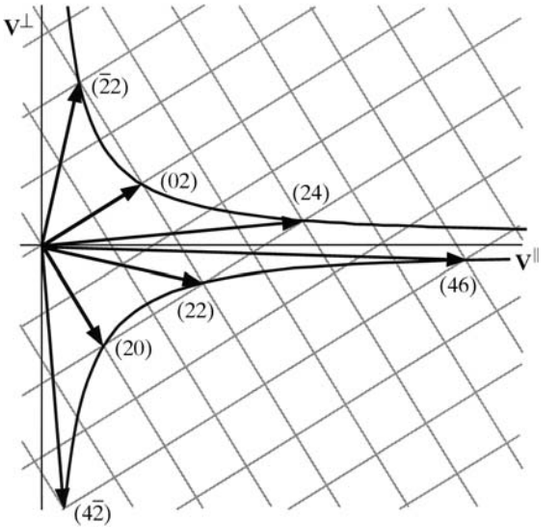

Fig. 4.6.3.11. Scaling operations of the Fibonacci sequence. The scaling operation S acts six times on the diffraction vector $\mathbf{H} = (4\bar{2})$ yielding the sequence $(4\bar{2}) \rightarrow (\bar{2}2) \rightarrow (20) \rightarrow (02) \rightarrow (22) \rightarrow (24) \rightarrow (46)$.

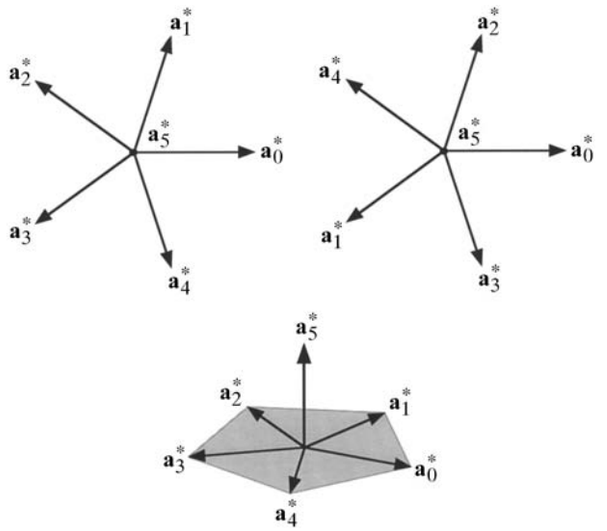

Fig. 4.6.3.12. Reciprocal basis of the decagonal phase in the 5D description projected upon $\mathbf{V}^{\parallel}$ (above left) and $\mathbf{V}^{\perp}$ (above right). Below, a perspective physical-space view is shown.

4.6.3.3.2. *Decagonal phases*

A structure quasiperiodic in two dimensions, periodic in the third dimension and with decagonal diffraction symmetry is called a decagonal phase. Its holohedral Laue symmetry group is $K = 10/mmm$. All reciprocal-space vectors $\mathbf{H} \in M^*$ can be represented on a basis (V basis) $\mathbf{a}_i^* = a_i^* (\cos 2\pi i/5, \sin 2\pi i/5, 0)$, $i = 1, \ldots, 4$ and $\mathbf{a}_5^* = a_5^*(0, 0, 1)$ (Fig. 4.6.3.12) as $\mathbf{H} = \sum_{i=1}^{5} h_i \mathbf{a}_i^*$. The vector components refer to a Cartesian coordinate system in physical (parallel) space. Thus, from the number of independent reciprocal-basis vectors necessary to index the Bragg reflections with integer numbers, the dimension of the embedding space has to be at least five. This can also be shown in a different way (Hermann, 1949).

The set M^* of all vectors $\mathbf{H}$ remains invariant under the action of the symmetry operators of the point group $10/mmm$. The symmetry-adapted matrix representations for the point-group generators, the tenfold rotation $\alpha = 10$, the reflection plane $\beta = m_2$ (normal of the reflection plane along the vectors $\mathbf{a}_i^* \mathbf{a}_{i+3}^*$ with $i = 1, \ldots, 4$ modulo 5) and the inversion operation $\Gamma(\gamma) = \bar{1}$ may be written in the form

$$\Gamma(\alpha) = \begin{pmatrix} 0 & 1 & \bar{1} & 0 & 0 \\ 0 & 1 & 0 & \bar{1} & 0 \\ 0 & 1 & 0 & 0 & 0 \\ \bar{1} & 1 & 0 & 0 & 0 \\ 0 & 0 & 0 & 0 & 1 \end{pmatrix}_D \quad \Gamma(\beta) = \begin{pmatrix} 0 & 0 & 0 & 1 & 0 \\ 0 & 0 & 1 & 0 & 0 \\ 0 & 1 & 0 & 0 & 0 \\ 1 & 0 & 0 & 0 & 0 \\ 0 & 0 & 0 & 0 & 1 \end{pmatrix}_D$$

$$\Gamma(\gamma) = \begin{pmatrix} \bar{1} & 0 & 0 & 0 & 0 \\ 0 & \bar{1} & 0 & 0 & 0 \\ 0 & 0 & \bar{1} & 0 & 0 \\ 0 & 0 & 0 & \bar{1} & 0 \\ 0 & 0 & 0 & 0 & \bar{1} \end{pmatrix}_D .$$

By block-diagonalization, these reducible symmetry matrices can be decomposed into non-equivalent irreducible representations. These can be assigned to the two orthogonal subspaces forming the 5D embedding space $\mathbf{V} = \mathbf{V}^{\parallel} \oplus \mathbf{V}^{\perp}$, the 3D parallel (physical) subspace $\mathbf{V}^{\parallel}$ and the perpendicular 2D subspace $\mathbf{V}^{\perp}$. Thus, using $W\Gamma W^{-1} = \Gamma_V = \Gamma_V^{\parallel} \oplus \Gamma_V^{\perp}$, we obtain

$$\Gamma_V(\alpha) = \left(\begin{array}{ccc|cc} \cos(\pi/5) & -\sin(\pi/5) & 0 & 0 & 0 \\ \sin(\pi/5) & \cos(\pi/5) & 0 & 0 & 0 \\ 0 & 0 & 1 & 0 & 0 \\ \hline 0 & 0 & 0 & \cos(3\pi/5) & -\sin(3\pi/5) \\ 0 & 0 & 0 & \sin(3\pi/5) & \cos(3\pi/5) \end{array}\right)_V$$

$$= \left(\begin{array}{c|c} \Gamma^{\parallel}(\alpha) & 0 \\ \hline 0 & \Gamma^{\perp}(\alpha) \end{array}\right)_V ,$$

$$\Gamma_V(\beta) = \left(\begin{array}{ccc|cc} 1 & 0 & 0 & 0 & 0 \\ 0 & \bar{1} & 0 & 0 & 0 \\ 0 & 0 & 1 & 0 & 0 \\ \hline 0 & 0 & 0 & \bar{1} & 0 \\ 0 & 0 & 0 & 0 & 1 \end{array}\right)_V , \quad \Gamma_V(\gamma) \left(\begin{array}{ccc|cc} \bar{1} & 0 & 0 & 0 & 0 \\ 0 & \bar{1} & 0 & 0 & 0 \\ 0 & 0 & \bar{1} & 0 & 0 \\ \hline 0 & 0 & 0 & \bar{1} & 0 \\ 0 & 0 & 0 & 0 & \bar{1} \end{array}\right)_V ,$$

where

$$W = \left(\begin{array}{ccccc} a_1^* \cos(2\pi/5) & a_2^* \cos(4\pi/5) & a_3^* \cos(6\pi/5) & a_4^* \cos(8\pi/5) & 0 \\ a_1^* \sin(2\pi/5) & a_2^* \sin(4\pi/5) & a_3^* \sin(6\pi/5) & a_4^* \sin(8\pi/5) & 0 \\ 0 & 0 & 0 & 0 & a_5^* \\ \hline a_1^* \cos(6\pi/5) & a_2^* \cos(2\pi/5) & a_3^* \cos(8\pi/5) & a_4^* \cos(4\pi/5) & 0 \\ a_1^* \sin(6\pi/5) & a_2^* \sin(2\pi/5) & a_3^* \sin(8\pi/5) & a_4^* \sin(4\pi/5) & 0 \end{array}\right).$$

The column vectors of the matrix W give the parallel- (above the partition line) and perpendicular-space components (below the partition line) of a reciprocal basis in V space. Thus, W can be rewritten using the physical-space reciprocal basis defined above as

$$W = (\, \mathbf{d}_1^*, \quad \mathbf{d}_2^*, \quad \mathbf{d}_3^*, \quad \mathbf{d}_4^*, \quad \mathbf{d}_5^* \,),$$

yielding the reciprocal basis $\mathbf{d}_i^*, i = 1, \ldots, 5$, in the 5D embedding space (D space):

$$\mathbf{d}_i^* = a_i^* \begin{pmatrix} \cos(2\pi i/5) \\ \sin(2\pi i/5) \\ 0 \\ \cos(6\pi i/5) \\ \sin(6\pi i/5) \end{pmatrix}_V , \; i = 1, \ldots, 4 \text{ and } \mathbf{d}_5^* = a_5^* \begin{pmatrix} 0 \\ 0 \\ 1 \\ 0 \\ 0 \end{pmatrix}_V .$$

The 5×5 symmetry matrices can each be decomposed into a 3×3 matrix and a 2×2 matrix. The first one, $\Gamma^{\parallel}$, acts on the parallel-space component, the second one, $\Gamma^{\perp}$, on the perpendicular-space component. In the case of $\Gamma(\alpha)$, the coupling factor between a rotation in parallel and perpendicular space is 3. Thus, a $\pi/5$ rotation in physical space is related to a $3\pi/5$ rotation in perpendicular space (Fig. 4.6.3.12).

With the condition $\mathbf{d}_i \cdot \mathbf{d}_j^* = \delta_{ij}$, a basis in direct 5D space is obtained:

$$\mathbf{d}_i = \frac{2}{5a_i^*} \begin{pmatrix} \cos(2\pi i/5) - 1 \\ \sin(2\pi i/5) \\ 0 \\ \cos(6\pi i/5) - 1 \\ \sin(6\pi i/5) \end{pmatrix}, \; i = 1, \ldots, 4, \text{ and } \mathbf{d}_5 = \frac{1}{a_5^*} \begin{pmatrix} 0 \\ 0 \\ 1 \\ 0 \\ 0 \end{pmatrix}.$$

The metric tensors G, G^* are of the type

$$\begin{pmatrix} A & C & C & C & 0 \\ C & A & C & C & 0 \\ C & C & A & C & 0 \\ C & C & C & A & 0 \\ 0 & 0 & 0 & 0 & B \end{pmatrix}$$

with $A = 2a_1^{*2}, B = a_5^{*2}, C = -(1/2)a_1^{*2}$ for the reciprocal space and $A = 4/5a_1^{*2}, B = 1/a_5^{*2}, C = 2/5a_1^{*2}$ for the direct space. Thus, for the lattice parameters in reciprocal space we obtain

$d_i^* = a_i^*(2)^{1/2}$, $i = 1, \ldots, 4$; $d_5^* = a_5^*$; $\alpha_{ij}^* = 104.5°$, $i,j = 1, \ldots, 4$; $\alpha_{i5}^* = 90°$, $i = 1, \ldots, 4$, and for those in direct space $d_i = 2/[a_i^*(5)^{1/2}]$, $i = 1, \ldots, 4$; $d_5 = 1/a_5^*$; $\alpha_{ij} = 60°$, $i,j = 1, \ldots, 4$; $\alpha_{i5} = 90°, i = 1, \ldots, 4$. The volume of the 5D unit cell can be calculated from the metric tensor G:

$$V = [\det(G)]^{1/2} = \frac{4}{5(5)^{1/2}(a_1^*)^4 a_5^*} = \frac{(5)^{1/2}}{4}(d_1)^4 d_5.$$

Since decagonal phases are only quasiperiodic in two dimensions, it is sufficient to demonstrate their characteristics on a 2D example, the canonical *Penrose tiling* (Penrose, 1974). It can be constructed from two unit tiles: a skinny (acute angle $\alpha_s = \pi/5$) and a fat (acute angle $\alpha_f = 2\pi/5$) rhomb with equal edge lengths a_r and areas $A_S = a_r^2 \sin(\pi/5)$, $A_F = a_r^2 \sin(2\pi/5)$ (Fig. 4.6.3.13). The areas and frequencies of these two unit tiles in the Penrose tiling are both in a ratio 1 to τ. By replacing each skinny and fat rhomb according to the inflation rule, a τ-inflated tiling is obtained. Inflation (deflation) means that the number of tiles is inflated (deflated), their edge lengths are decreased (increased) by a factor τ. By infinite repetition of this inflation operation, an infinite Penrose tiling is generated. Consequently, this substitution operation leaves the tiling invariant.

From Fig. 4.6.3.13 it can be seen that the sets of vertices of the deflated tilings are subsets of the set of vertices of the original tiling. The τ-deflated tiling is dual to the original tiling; a further deflation by a factor τ gives the original tiling again. However, the edge lengths of the tiles are increased by a factor τ^2, and the tiling is rotated around 36°. Only the fourth deflation of the original tiling yields the original tiling in its original orientation but with all lengths multiplied by a factor τ^4.

Contrary to the reciprocal-space scaling behaviour of $M^* = \{\mathbf{H}^{\parallel} = \sum_{i=1}^4 h_i \mathbf{a}_i^* | h_i \in \mathbb{Z}\}$, the set of vertices $M = \{\mathbf{r} = \sum_{i=1}^4 n_i \mathbf{a}_i | n_i \in \mathbb{Z}\}$ of the Penrose tiling is not invariant by scaling the length scale simply by a factor τ using the scaling matrix S:

$$S = \begin{pmatrix} 0 & 1 & 0 & \bar{1} \\ 0 & 1 & 1 & \bar{1} \\ \bar{1} & 1 & 1 & 0 \\ \bar{1} & 0 & 1 & 0 \end{pmatrix}_D \text{ acting on vectors } \mathbf{r} = \begin{pmatrix} n_1 \\ n_2 \\ n_3 \\ n_4 \end{pmatrix}_D .$$

The square of S, however, maps all vertices of the Penrose tiling upon other ones:

$$S^2 = \begin{pmatrix} 1 & 1 & 0 & \bar{1} \\ 0 & 2 & 1 & \bar{1} \\ \bar{1} & 1 & 2 & 0 \\ \bar{1} & 0 & 1 & 1 \end{pmatrix}_D , \quad \Gamma(\alpha)S^2 = \begin{pmatrix} 1 & 1 & \bar{1} & \bar{1} \\ 1 & 2 & 0 & \bar{2} \\ 0 & 2 & 1 & \bar{1} \\ \bar{1} & 1 & 1 & 0 \end{pmatrix}_D .$$

S^2 corresponds to a hyperbolic rotation with $\chi = \cosh^{-1}(3/2)$ in superspace (Janner, 1992). However, only operations of the type S^{4n}, $n = 0, 1, 2 \ldots$, scale the Penrose tiling in a way which is equivalent to the ($4n$th) substitutional operations discussed above. The rotoscaling operation $\Gamma(\alpha)S^2$, also a symmetry operation of the Penrose tiling, leaves a pentagram invariant as demonstrated in Fig. 4.6.3.14 (Janner, 1992). Block-diagonalization of the scaling matrix S decomposes it into two non-equivalent irreducible representations which give the scaling properties in the two orthogonal subspaces of the 4D embedding space, $\mathbf{V} = \mathbf{V}^{\parallel} \oplus \mathbf{V}^{\perp}$, the 2D parallel (physical) subspace $\mathbf{V}^{\parallel}$ and the perpendicular 2D subspace $\mathbf{V}^{\perp}$. Thus, using $WSW^{-1} = S_V = S_V^{\parallel} \oplus S_V^{\perp}$, we obtain

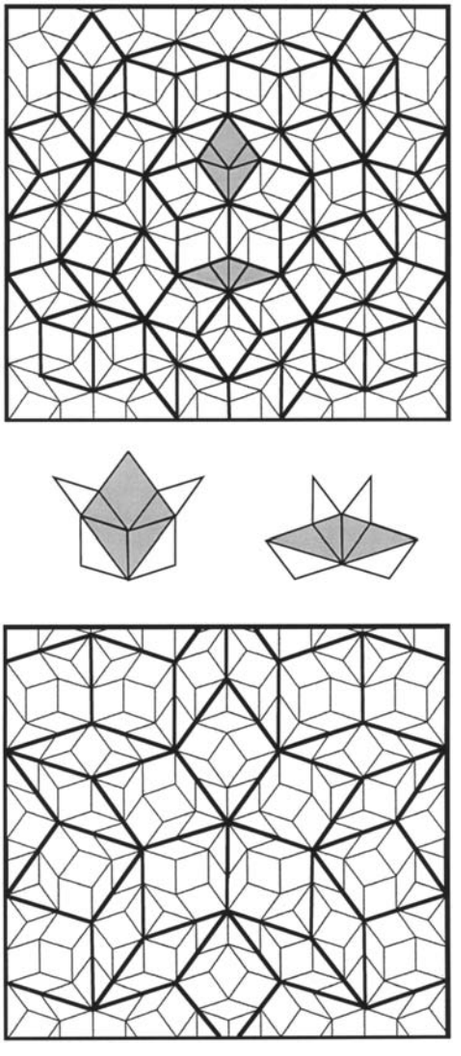

Fig. 4.6.3.13. A section of a Penrose tiling (thin lines) superposed by its τ-deflated tiling (above, thick lines) and by its τ^2-deflated tiling (below, thick lines). In the middle, the inflation rule of the Penrose tiling is illustrated.

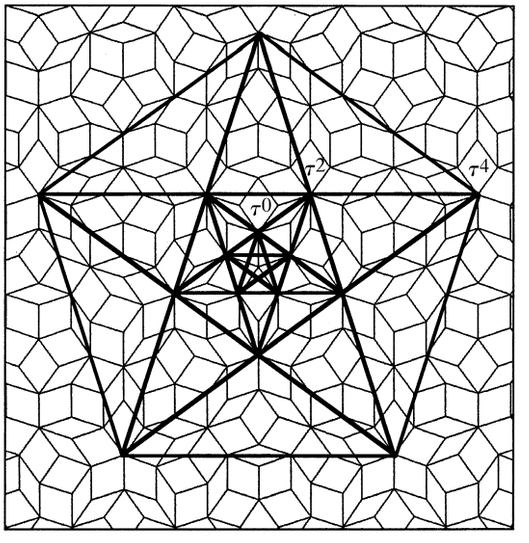

Fig. 4.6.3.14. Scaling symmetry of a pentagram superposed on the Penrose tiling. A vector pointing to a corner of a pentagon (star) is mapped by the rotoscaling operation (rotation around $\pi/5$ and dilatation by a factor τ^2) onto the next largest pentagon (star).

$$S_V = \left(\begin{array}{cc|cc} \tau & 0 & 0 & 0 \\ 0 & \tau & 0 & 0 \\ \hline 0 & 0 & -1/\tau & 0 \\ 0 & 0 & 0 & -1/\tau \end{array}\right)_V = \left(\begin{array}{c|c} S_V^{\parallel} & 0 \\ \hline 0 & S_V^{\perp} \end{array}\right)_V,$$

where

$$W = \left(\begin{array}{cccc} a_1^* \cos(2\pi/5) & a_2^* \cos(4\pi/5) & a_3^* \cos(6\pi/5) & a_4^* \cos(8\pi/5) \\ a_1^* \sin(2\pi/5) & a_2^* \sin(4\pi/5) & a_3^* \sin(6\pi/5) & a_4^* \sin(8\pi/5) \\ \hline a_1^* \cos(4\pi/5) & a_2^* \cos(8\pi/5) & a_3^* \cos(2\pi/5) & a_4^* \cos(6\pi/5) \\ a_1^* \sin(4\pi/5) & a_2^* \sin(8\pi/5) & a_3^* \sin(2\pi/5) & a_4^* \sin(6\pi/5) \end{array}\right).$$

The 2D Penrose tiling can also be embedded canonically in the 5D space. Canonically means that the 5D lattice is hypercubic and that the projection of one unit cell upon the 3D perpendicular space $\mathbf{V}^{\perp}$, giving a rhomb-icosahedron, defines the atomic surface. However, the parallel-space image $\mathbf{a}_i^*$, $i = 1, \ldots, 4$, with $\mathbf{a}_0^* = -(\mathbf{a}_1^* + \mathbf{a}_2^* + \mathbf{a}_3^* + \mathbf{a}_4^*)$, of the 5D basis $\mathbf{d}_i^*, i = 1, \ldots, 4$ is not linearly independent. Consequently, the atomic surface consists of only a subset of the points contained in the rhomb-icosahedron: five equidistant pentagons (one with diameter zero) resulting as sections of the rhomb-icosahedron with five equidistant parallel planes (Fig. 4.6.3.15). The linear dependence of the 5D basis allows the embedding in the 4D space. The resulting hyper-rhombohedral hyperlattice is spanned by the basis $\mathbf{d}_i$, $i = 1, \ldots, 4$, discussed above. The atomic surfaces occupy the positions $p/5(1111)$, $p = 1, \ldots, 4$, on the body diagonal of the 4D unit cell. Neighbouring pentagons are in an *anti* position to each other (Fig. 4.6.3.16). Thus the 4D unit cell is decorated centrosymmetrically. The edge length a_r of a Penrose rhomb is related to the length of physical-space basis vectors a_i^* by $a_r = \tau S$, with the smallest distance $S = (2\tau/5a_i^*), i = 1, \ldots, 4$. The *point density* (number of vertices per unit area) of a Penrose tiling with Penrose rhombs of edge length a_r can be calculated from the ratio of the relative number of unit tiles in the tiling to their area:

$$\rho = \frac{1+\tau}{a_r^2[\sin(\pi/5) + \tau \sin(2\pi/5)]} = (5/2)a_i^{*2}(2-\tau)^2 \tan(2\pi/5).$$

This is equivalent to the calculation from the 4D description,

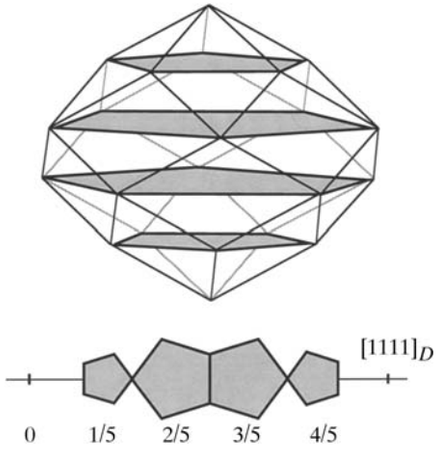

Fig. 4.6.3.15. Atomic surface of the Penrose tiling in the 5D hypercubic description. The projection of the 5D hypercubic unit cell upon $\mathbf{V}^{\perp}$ gives a rhomb-icosahedron (above). The Penrose tiling is generated by four equidistant pentagons (shaded) inscribed in the rhomb-icosahedron. Below is a perpendicular-space projection of the same pentagons, which are located on the $[1111]_D$ diagonal of the 4D hyper-rhombohedral unit cell in the 4D description.

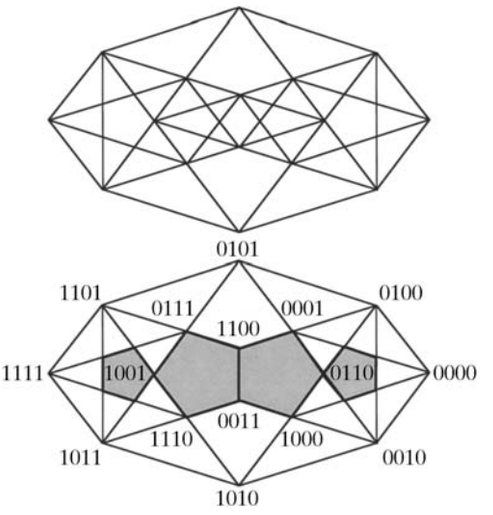

Fig. 4.6.3.16. Projection of the 4D hyper-rhombohedral unit cell of the Penrose tiling in the 4D description upon the perpendicular space. In the upper drawing all edges between the 16 corners are shown. In the lower drawing the corners are indexed and the four pentagonal atomic surfaces of the Penrose tiling are shaded.

$$\rho = \frac{\sum_{i=1}^{4} \Omega_{\rm AS}^i}{\Omega_{\rm UC}} = \frac{\sum_{i=1}^{4} (5/2)\lambda^2 \sin(2\pi/5)}{4/[5(5)^{1/2}|a_i^*|^4]} = (5/2)a_i^{*2}(2-\tau)^2 \tan(2\pi/5),$$

where $\Omega_{\rm AS}$ and $\Omega_{\rm UC}$ are the area of the atomic surface and the volume of the 4D unit cell, respectively. The pentagon radii are $\lambda_{1,4} = 2(2-\tau)/5a^*$ and $\lambda_{2,3} = 2(\tau-1)/5a^*$ for the atomic surfaces in $(p/5)(1111)$ with $p = 1, 4$ and $p = 2, 3$. A detailed discussion of the properties of Penrose tiling is given in the papers of Penrose (1974, 1979), Jaric (1986) and Pavlovitch & Kleman (1987).

4.6.3.3.2.1. *Indexing*

The indexing of the submodule M_1^* of the diffraction pattern of a decagonal phase is not unique. Since M_1^* corresponds to a $\mathbb{Z}$ module of rank 4 with decagonal point symmetry, it is invariant under scaling by $\tau^n, n \in \mathbb{Z}$: $S^n M^* = \tau^n M^*$. Nevertheless, an optimum basis (low indices are assigned to strong reflections) can be derived: not the metrics, as for regular periodic crystals, but the intensity distribution characterizes the best choice of indexing.

A correct set of reciprocal-basis vectors can be identified experimentally in the following way:

(1) Find directions of systematic absences or pseudo-absences determining the possible orientations of the reciprocal-basis vectors (see Rabson *et al.*, 1991).

(2) Find pairs of strong reflections whose physical-space diffraction vectors are related to each other by the factor τ.

(3) Index these reflections by assigning an appropriate value to a^*. This value should be derived from the shortest interatomic distance S and the edge length of the unit tiles expected in the structure.

(4) The reciprocal basis is correct if all observable Bragg reflections can be indexed with integer numbers.

4.6.3.3.2.2. *Diffraction symmetry*

The diffraction symmetry of decagonal phases can be described by the Laue groups $10/mmm$ or $10/m$. The set of all vectors $\mathbf{H}$ forms a Fourier module $M^* = \{\mathbf{H}^{\parallel} = \sum_{i=1}^{5} h_i \mathbf{a}_i^* | h_i \in \mathbb{Z}\}$ of rank 5 in physical space which can be decomposed into two submodules

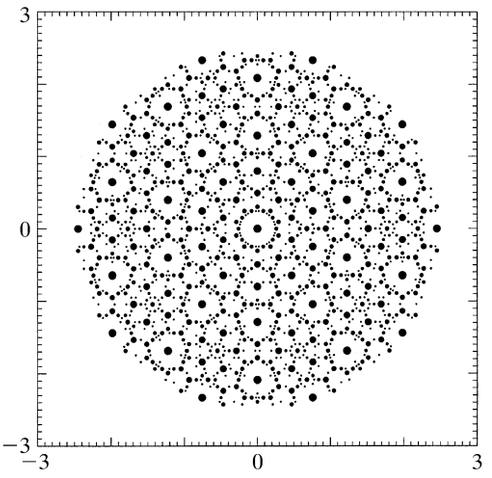

Fig. 4.6.3.17. Schematic diffraction pattern of the Penrose tiling (edge length of the Penrose unit rhombs $a_r = 4.04$ Å). All reflections are shown within $10^{-2}|F(\mathbf{0})|^2 < |F(\mathbf{H})|^2 < |F(\mathbf{0})|^2$ and $0 \leq |\mathbf{H}^{\parallel}| \leq 2.5$ Å^{-1}.

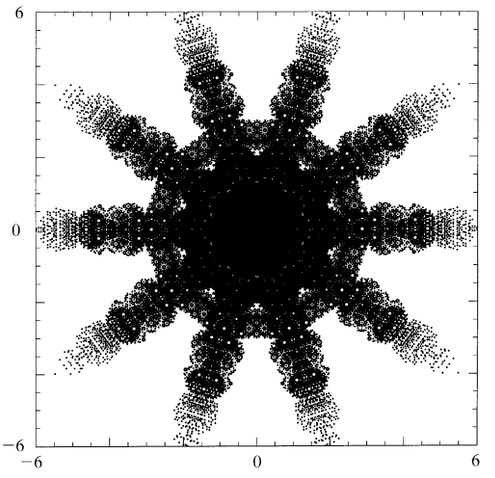

Fig. 4.6.3.19. The perpendicular-space diffraction pattern of the Penrose tiling (edge length of the Penrose unit rhombs $a_r = 4.04$ Å). All reflections are shown within $10^{-4}|F(\mathbf{0})|^2 < |F(\mathbf{H})|^2 < |F(\mathbf{0})|^2$ and $0 \leq |\mathbf{H}^{\parallel}| \leq 2.5$ Å^{-1}.

$M^* = M_1^* \oplus M_2^*$. $M_1^* = \{h_1\mathbf{a}_1^* + h_2\mathbf{a}_2^* + h_3\mathbf{a}_3^* + h_4\mathbf{a}_4^*\}$ corresponds to a $\mathbb{Z}$ module of rank 4 in a 2D subspace, $M_2^* = \{h_5\mathbf{a}_5^*\}$ corresponds to a $\mathbb{Z}$ module of rank 1 in a 1D subspace. Consequently, the first submodule can be considered as a projection from a 4D reciprocal lattice, $M_1^* = \pi^{\parallel}(\Sigma^*)$, while the second submodule is of the form of a regular 1D reciprocal lattice, $M_2^* = \Lambda^*$. The diffraction pattern of the Penrose tiling decorated with equal point scatterers on its vertices is shown in Fig. 4.6.3.17. All Bragg reflections within $10^{-2}|F(\mathbf{0})|^2 < |F(\mathbf{H})|^2 < |F(\mathbf{0})|^2$ are depicted. Without intensity-truncation limit, the diffraction pattern would be densely filled with discrete Bragg reflections. To illustrate their spatial and intensity distribution, an enlarged section of Fig. 4.6.3.17 is shown in Fig. 4.6.3.18. This picture shows all Bragg reflections within $10^{-4}|F(\mathbf{0})|^2 < |F(\mathbf{H})|^2 < |F(\mathbf{0})|^2$. The projected 4D reciprocal-lattice unit cell is drawn and several reflections are indexed. All reflections are arranged along lines in five symmetry-equivalent orientations. The perpendicular-space diffraction patterns (Figs. 4.6.3.19 and 4.6.3.20) show a characteristic star-like distribution of the Bragg reflections. This is a consequence of the pentagonal shape of the atomic surfaces: the Fourier transform of a pentagon has a star-like distribution of strong Fourier coefficients.

The 5D decagonal space groups that may be of relevance for the description of decagonal phases are listed in Table 4.6.3.1. These space groups are a subset of all 5D decagonal space groups fulfilling the condition that the 5D point groups they are associated with are isomorphous to the 3D point groups describing the diffraction symmetry. Their structures are comparable to 3D hexagonal groups. Hence, only primitive lattices exist. The orientation of the symmetry elements in the 5D space is defined by the isomorphism of the 3D and 5D point groups. However, the action of the tenfold rotation is different in the subspaces $\mathbf{V}^{\parallel}$ and $\mathbf{V}^{\perp}$: a rotation of $\pi/5$ in $\mathbf{V}^{\parallel}$ is correlated with a rotation of $3\pi/5$ in $\mathbf{V}^{\perp}$. The reflection and inversion operations are equivalent in both subspaces.

4.6.3.3.2.3. *Structure factor*

The structure factor for the decagonal phase corresponds to the Fourier transform of the 5D unit cell,

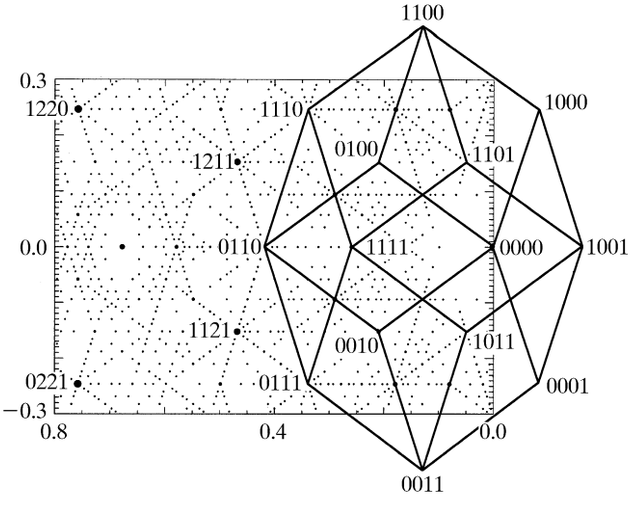

Fig. 4.6.3.18. Enlarged section of Fig. 4.6.3.17. All reflections shown are selected within the given limits from a data set within $10^{-4}|F(\mathbf{0})|^2 < |F(\mathbf{H})|^2 < |F(\mathbf{0})|^2$ and $0 \leq |\mathbf{H}^{\parallel}| \leq 2.5$ Å^{-1}. The projected 4D reciprocal-lattice unit cell is drawn and several reflections are indexed.

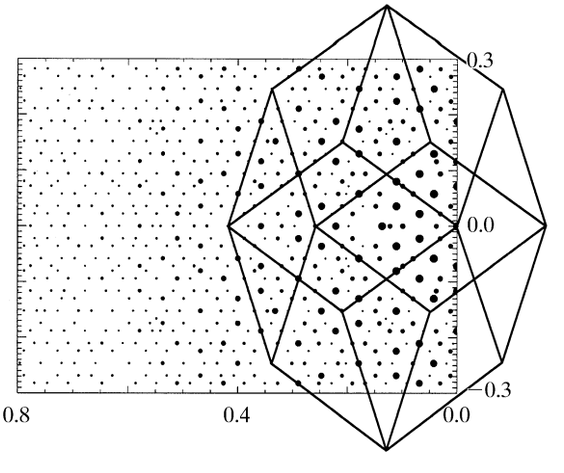

Fig. 4.6.3.20. Enlarged section of Fig. 4.6.3.19 showing the projected 4D reciprocal-lattice unit cell.

Table 4.6.3.1. *3D point groups of order k describing the diffraction symmetry and corresponding 5D decagonal space groups with reflection conditions (see Rabson et al., 1991)*

3D point group	k	5D space group	Reflection condition
$\frac{10}{m}\frac{2}{m}\frac{2}{m}$	40	$P\frac{10}{m}\frac{2}{m}\frac{2}{m}$	No condition
		$P\frac{10}{m}\frac{2}{c}\frac{2}{c}$	$h_1h_2h_2h_1h_5 : h_5 = 2n$ $h_1h_2\overline{h_2h_1}h_5 : h_5 = 2n$
		$P\frac{10_5}{m}\frac{2}{m}\frac{2}{c}$	$h_1h_2\overline{h_2h_1}h_5 : h_5 = 2n$
		$P\frac{10_5}{m}\frac{2}{c}\frac{2}{m}$	$h_1h_2h_2h_1h_5 : h_5 = 2n$
$\frac{10}{m}$	20	$P\frac{10}{m}$	No condition
		$P\frac{10_5}{m}$	$0000h_5 : h_5 = 2n$
1022	20	$P1022$	No condition
		$P10_j22$	$0000h_5 : jh_5 = 10n$
$10mm$	20	$P10mm$	No condition
		$P10cc$	$h_1h_2h_2h_1h_5 : h_5 = 2n$ $h_1h_2\overline{h_2h_1}h_5 : h_5 = 2n$
		$P10_5mc$	$h_1h_2\overline{h_2h_1}h_5 : h_5 = 2n$
		$P10_5cm$	$h_1h_2h_2h_1h_5 : h_5 = 2n$
$\overline{1}0m2$	20	$P\overline{1}0m2$	No condition
		$P\overline{1}0c2$	$h_1h_2h_2h_1h_5 : h_5 = 2n$
		$P\overline{1}02m$	No condition
		$P\overline{1}02c$	$h_1h_2\overline{h_2h_1}h_5 : h_5 = 2n$
10	10	$P10$	No condition
		$P10_j$	$0000h_5 : jh_5 = 10n$

$$F(\mathbf{H}) = \sum_{k=1}^{N} f_k(\mathbf{H}^{\parallel}) T_k(\mathbf{H}^{\parallel}, \mathbf{H}^{\perp}) g_k(\mathbf{H}^{\perp}) \exp(2\pi i \mathbf{H}\cdot\mathbf{r}_k),$$

with 5D diffraction vectors $\mathbf{H} = \sum_{i=1}^{5} h_i \mathbf{d}_i^*$, N hyperatoms, parallel-space atomic scattering factor $f_k(\mathbf{H}^{\parallel})$, temperature factor $T_k(\mathbf{H}^{\parallel}, \mathbf{H}^{\perp})$ and perpendicular-space geometric form factor $g_k(\mathbf{H}^{\perp})$. $T_k(\mathbf{H}^{\parallel}, \mathbf{0})$ is equivalent to the conventional Debye–Waller factor and $T_k(\mathbf{0}, \mathbf{H}^{\perp})$ describes random fluctuations along the perpendicular-space coordinate. These fluctuations cause characteristic jumps of vertices in physical space (*phason flips*). Even random phason flips map the vertices onto positions which can still be described by physical-space vectors of the type $\mathbf{r} = \sum_{i=1}^{5} n_i \mathbf{a}_i$. Consequently, the set $M = \{\mathbf{r} = \sum_{i=1}^{5} n_i \mathbf{a}_i | n_i \in \mathbb{Z}\}$ of all possible vectors forms a $\mathbb{Z}$ module. The shape of the atomic surfaces corresponds to a selection rule for the positions actually occupied. The geometric form factor $g_k(\mathbf{H}^{\perp})$ is equivalent to the Fourier transform of the *atomic surface*, *i.e.* the 2D perpendicular-space component of the 5D *hyperatoms*.

For example, the canonical Penrose tiling $g_k(\mathbf{H}^{\perp})$ corresponds to the Fourier transform of pentagonal atomic surfaces:

$$g_k(\mathbf{H}^{\perp}) = (1/A_{\rm UC}^{\perp}) \int_{A_k} \exp(2\pi i \mathbf{H}^{\perp}\cdot\mathbf{r})\, \mathrm{d}\mathbf{r},$$

where $A_{\rm UC}^{\perp}$ is the area of the 5D unit cell projected upon $\mathbf{V}^{\perp}$ and A_k is the area of the kth atomic surface. The area $A_{\rm UC}^{\perp}$ can be calculated using the formula

$$A_{\rm UC}^{\perp} = (4/25a_i^{*2})[(7+\tau)\sin(2\pi/5) + (2+\tau)\sin(4\pi/5)].$$

Evaluating the integral by decomposing the pentagons into triangles, one obtains

$$g_k(\mathbf{H}^{\perp}) = \frac{1}{A_{\rm UC}^{\perp}} \sin\left(\frac{2\pi}{5}\right) \times \sum_{j=0}^{4} \frac{A_j[\exp(iA_{j+1}\lambda_k) - 1] - A_{j+1}[\exp(iA_j\lambda_k) - 1]}{A_jA_{j+1}(A_j - A_{j+1})}$$

with $j = 0, \ldots, 4$ running over the five triangles, where the radii of the pentagons are λ_j, $A_j = 2\pi\mathbf{H}^{\perp}\mathbf{e}_j$,

$$\mathbf{H}^{\perp} = \pi^{\perp}(\mathbf{H}) = \sum_{j=0}^{4} h_j a_j^* \begin{pmatrix} 0 \\ 0 \\ 0 \\ \cos(6\pi j/5) \\ \sin(6\pi j/5) \end{pmatrix}$$

and the vectors

$$\mathbf{e}_j = \frac{1}{a_j^*} \begin{pmatrix} 0 \\ 0 \\ 0 \\ \cos(2\pi j/5) \\ \sin(2\pi j/5) \end{pmatrix} \text{ with } j = 0, \ldots, 4.$$

As shown by Ishihara & Yamamoto (1988), the Penrose tiling can be considered to be a superstructure of a pentagonal tiling with only one type of pentagonal atomic surface in the nD unit cell. Thus, for the Penrose tiling, three special reflection classes can be distinguished: for $|\sum_{i=1}^{4} h_i| = m \bmod 5$ and $m = 0$ the class of strong main reflections is obtained, and for $m = \pm 1, \pm 2$ the classes of weaker first- and second-order satellite reflections are obtained (see Fig. 4.6.3.18).

4.6.3.3.2.4. *Intensity statistics*

This section deals with the reciprocal-space characteristics of the 2D quasiperiodic component of the 3D structure, namely the Fourier module M_1^*. The radial structure-factor distributions of the Penrose tiling decorated with point scatterers are plotted in Figs. 4.6.3.21 and 4.6.3.22 as a function of parallel and perpendicular space. The distribution of $|F(\mathbf{H})|$ as a function of their frequencies clearly resembles a centric distribution, as can be expected from the centrosymmetric 4D subunit cell. The shape of the distribution function depends on the radius of the limiting sphere in reciprocal space. The number of weak reflections increases to the power of four, that of strong reflections only quadratically (strong reflections always have small $\mathbf{H}^{\perp}$ components). The radial distribution of the structure-factor amplitudes as a function of perpendicular space clearly shows three branches, corresponding to the reflection classes $\sum_{i=1}^{4} h_i = m \bmod 5$ with $|m| = 0$, $|m| = 1$ and $|m| = 2$ (Fig. 4.6.3.23).

The weighted reciprocal space of the Penrose tiling contains an infinite number of Bragg reflections within a limited region of the physical space. Contrary to the diffraction pattern of a periodic structure consisting of point atoms on the lattice nodes, the Bragg reflections show intensities depending on the perpendicular-space components of their diffraction vectors (Figs. 4.6.3.19, 4.6.3.20 and 4.6.3.22).

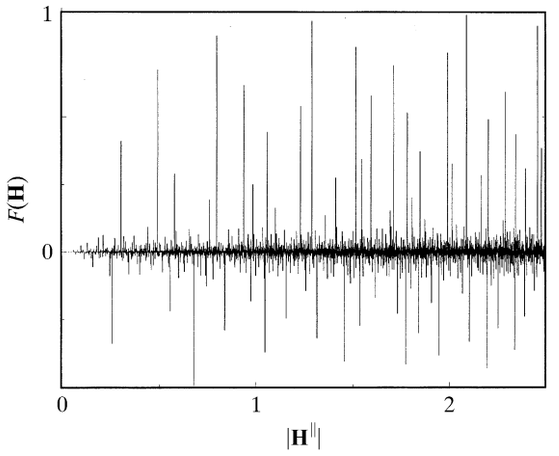

Fig. 4.6.3.21. Radial distribution function of the structure factors $F(\mathbf{H})$ of the Penrose tiling (edge length of the Penrose unit rhombs $a_r = 4.04$ Å) decorated with point atoms as a function of $\mathbf{H}^{\parallel}$. All structure factors within $10^{-4}|F(\mathbf{0})|^2 < |F(\mathbf{H})|^2 < |F(\mathbf{0})|^2$ and $0 \le |\mathbf{H}^{\parallel}| \le 2.5$ Å^{-1} have been used and normalized to $F(0000) = 1$.

4.6.3.3.2.5. *Relationships between structure factors at symmetry-related points of the Fourier image*

Scaling the Penrose tiling by a factor τ^{-n} by employing the matrix S^{-n} scales at the same time its reciprocal space by a factor τ^n:

$$S\mathbf{H} = \begin{pmatrix} 0 & 1 & 0 & \bar{1} & 0 \\ 0 & 1 & 1 & \bar{1} & 0 \\ \bar{1} & 1 & 1 & 0 & 0 \\ \bar{1} & 0 & 1 & 0 & 0 \\ 0 & 0 & 0 & 0 & 1 \end{pmatrix}_D \begin{pmatrix} h_1 \\ h_2 \\ h_3 \\ h_4 \\ h_5 \end{pmatrix} = \begin{pmatrix} h_2 - h_4 \\ h_2 + h_3 - h_4 \\ -h_1 + h_2 + h_3 \\ -h_1 + h_3 \\ h_5 \end{pmatrix}.$$

Since this operation increases the lengths of the diffraction vectors by the factor τ in parallel space and decreases them by the factor $1/\tau$ in perpendicular space, the following distribution of structure-factor magnitudes (for point atoms at rest) is obtained:

$$|F(S^n\mathbf{H})| > \left|F(S^{n-1}\mathbf{H})\right| > \ldots > \left|F(S^1\mathbf{H})\right| > |F(\mathbf{H})|,$$
$$\left|F(\tau^n\mathbf{H}^{\parallel})\right| > \left|F(\tau^{n-1}\mathbf{H}^{\parallel})\right| > \ldots > \left|F(\tau\mathbf{H}^{\parallel})\right| > |F(\mathbf{H})|.$$

The scaling operations S^n, $n \in \mathbb{Z}$, the rotoscaling operations $(\Gamma(\alpha)S^2)^n$ (Fig. 4.6.3.14) and the tenfold rotation $(\Gamma(\alpha))^n$, where

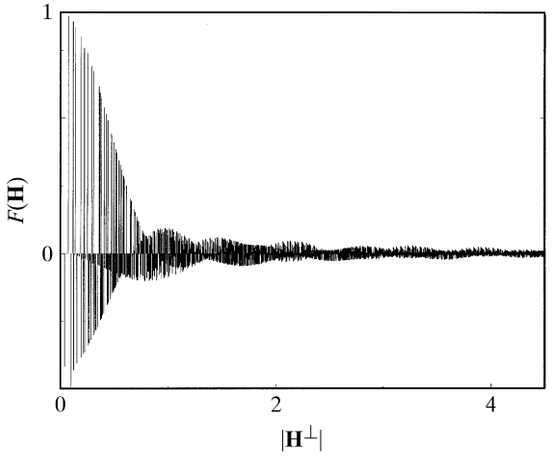

Fig. 4.6.3.22. Radial distribution function of the structure factors $F(\mathbf{H})$ of the Penrose tiling (edge length of the Penrose unit rhombs $a_r = 4.04$ Å) decorated with point atoms as a function of $\mathbf{H}^{\perp}$. All structure factors within $10^{-4}|F(\mathbf{0})|^2 < |F(\mathbf{H})|^2 < |F(\mathbf{0})|^2$ and $0 \le |\mathbf{H}^{\parallel}| \le 2.5$ Å^{-1} have been used and normalized to $F(0000) = 1$.

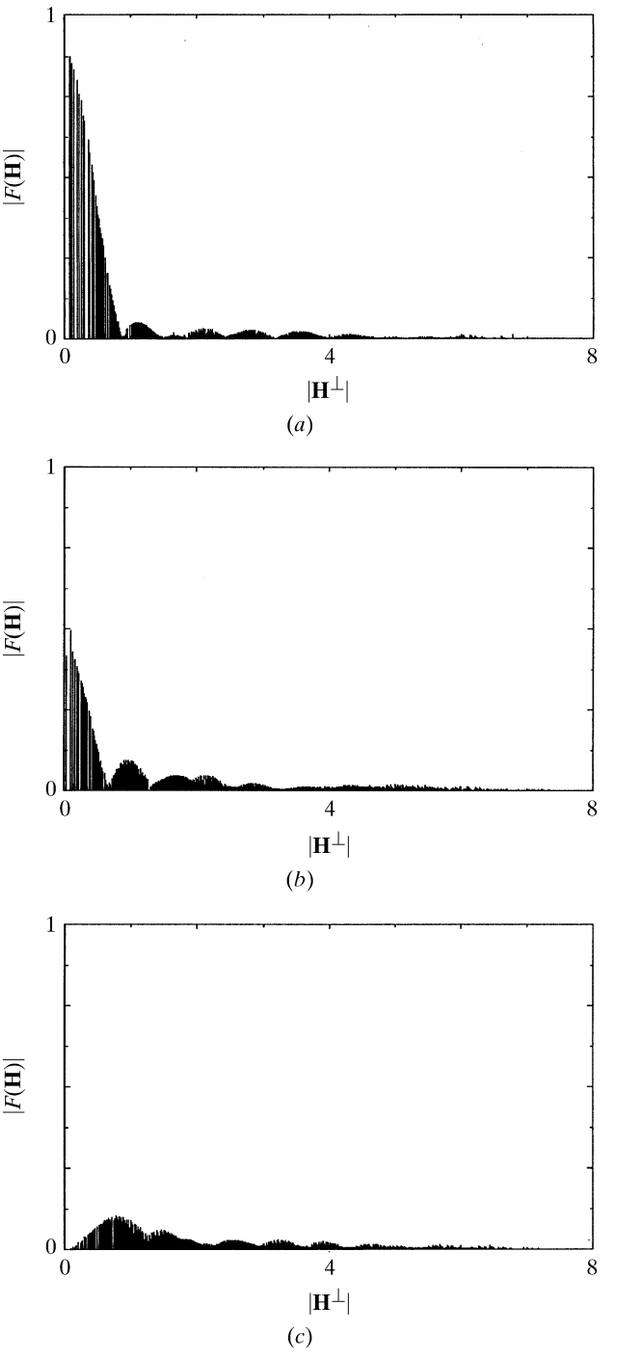

Fig. 4.6.3.23. Radial distribution function of the structure-factor magnitudes $|F(\mathbf{H})|$ of the Penrose tiling (edge length of the Penrose unit rhombs $a_r = 4.04$ Å) decorated with point atoms as a function of $\mathbf{H}^{\perp}$. All structure factors within $10^{-4}|F(\mathbf{0})|^2 < |F(\mathbf{H})|^2 < |F(\mathbf{0})|^2$ and $0 \le |\mathbf{H}^{\parallel}| \le 2.5$ Å^{-1} have been used and normalized to $F(0000) = 1$. The branches with (*a*) $\left|\sum_{i=1}^4 h_i\right| = 0 \bmod 5$, (*b*) $\left|\sum_{i=1}^4 h_i\right| = 1 \bmod 5$ and (*c*) $\left|\sum_{i=1}^4 h_i\right| = 2 \bmod 5$ are shown.

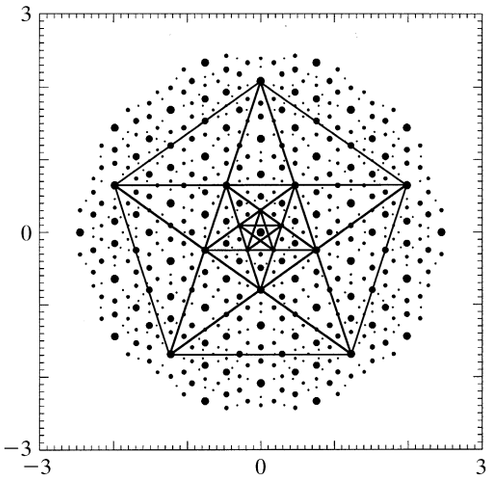

Fig. 4.6.3.24. Pentagrammal relationships between scaling symmetry-related positive structure factors $F(\mathbf{H})$ of the Penrose tiling (edge length $a_r = 4.04$ Å) in parallel space. The magnitudes of the structure factors are indicated by the diameters of the filled circles.

$$(\Gamma(\alpha)S^2)^n = \begin{pmatrix} 1 & 1 & \bar{1} & \bar{1} & 0 \\ 1 & 2 & 0 & \bar{2} & 0 \\ 0 & 2 & 1 & \bar{1} & 0 \\ \bar{1} & 1 & 1 & 0 & 0 \\ 0 & 0 & 0 & 0 & 1 \end{pmatrix}_D^n ,$$

connect all structure factors with diffraction vectors pointing to the nodes of an infinite series of pentagrams. The structure factors with positive signs are predominantly on the vertices of the pentagram while the ones with negative signs are arranged on circles around the vertices (Figs. 4.6.3.24 to 4.6.3.27).

4.6.3.3.3. *Icosahedral phases*

A structure that is quasiperiodic in three dimensions and exhibits icosahedral diffraction symmetry is called an icosahedral phase. Its holohedral Laue symmetry group is $K = m\bar{3}\bar{5}$. All reciprocal-space vectors $\mathbf{H} = \sum_{i=1}^{6} h_i \mathbf{a}_i^* \in M^*$ can be represented on a basis $\mathbf{a}_1^* = a^*(0,0,1)$, $\mathbf{a}_i^* = a^*[\sin\theta\cos(2\pi i/5), \sin\theta\sin(2\pi i/5), \cos\theta]$, $i = 2, \ldots, 6$ where $\sin\theta = 2/(5)^{1/2}$, $\cos\theta = 1/(5)^{1/2}$ and $\theta \simeq 63.44°$, the angle between two neighbouring fivefold axes (Fig. 4.6.3.28). This can be rewritten as

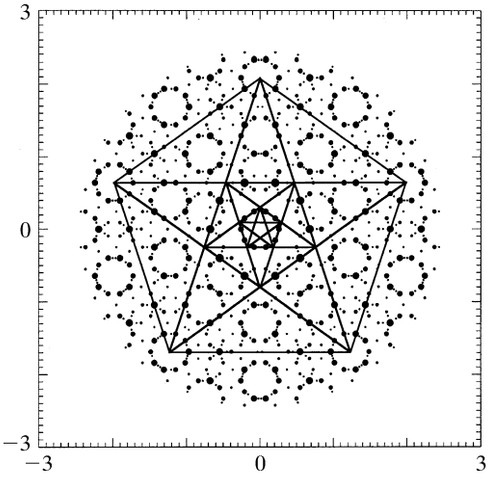

Fig. 4.6.3.25. Pentagrammal relationships between scaling symmetry-related negative structure factors $F(\mathbf{H})$ of the Penrose tiling (edge length $a_r = 4.04$ Å) in parallel space. The magnitudes of the structure factors are indicated by the diameters of the filled circles.

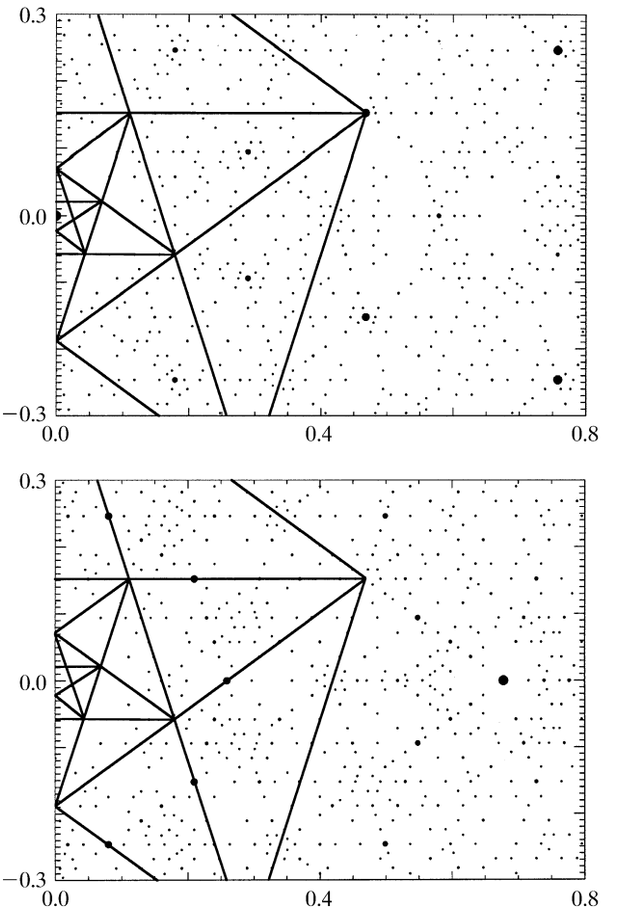

Fig. 4.6.3.26. Pentagrammal relationships between scaling symmetry-related structure factors $F(\mathbf{H})$ of the Penrose tiling (edge length $a_r = 4.04$ Å) in parallel space. Enlarged sections of Figs. 4.6.3.24 (above) and 4.6.3.25 (below) are shown.

$$\begin{pmatrix} \mathbf{a}_1^* \\ \mathbf{a}_2^* \\ \mathbf{a}_3^* \\ \mathbf{a}_4^* \\ \mathbf{a}_5^* \\ \mathbf{a}_6^* \end{pmatrix} = a^* \begin{pmatrix} 0 & 0 & 1 \\ \sin\theta\cos(4\pi/5) & \sin\theta\sin(4\pi/5) & \cos\theta \\ \sin\theta\cos(6\pi/5) & \sin\theta\sin(6\pi/5) & \cos\theta \\ \sin\theta\cos(8\pi/5) & \sin\theta\sin(8\pi/5) & \cos\theta \\ \sin\theta & 0 & \cos\theta \\ \sin\theta\cos(2\pi/5) & \sin\theta\sin(2\pi/5) & \cos\theta \end{pmatrix} \begin{pmatrix} \mathbf{e}_1^V \\ \mathbf{e}_2^V \\ \mathbf{e}_3^V \end{pmatrix},$$

where $\mathbf{e}_i^V$ are Cartesian basis vectors. Thus, from the number of independent reciprocal-basis vectors needed to index the Bragg reflections with integer numbers, the dimension of the embedding space has to be six. The vector components refer to a Cartesian coordinate system (V basis) in the physical (parallel) space.

The set $M^* = \{\mathbf{H}^{\parallel} = \sum_{i=1}^{6} h_i \mathbf{a}_i^* | h_i \in \mathbb{Z}\}$ of all diffraction vectors remains invariant under the action of the symmetry operators of the icosahedral point group $K = m\bar{3}\bar{5}$. The symmetry-adapted matrix representations for the point-group generators, one fivefold rotation α, a threefold rotation β and the inversion operation γ, can be written in the form

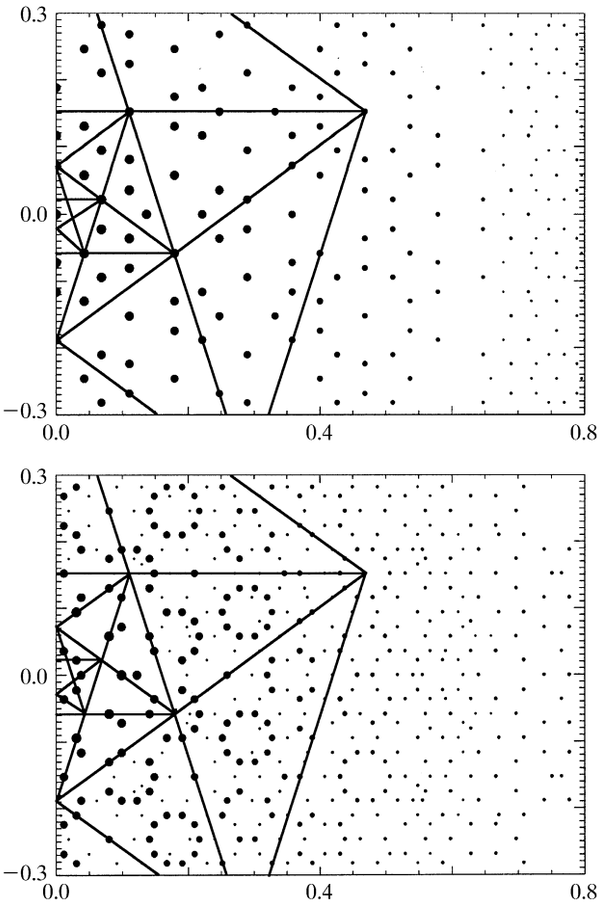

Fig. 4.6.3.27. Pentagrammal relationships between scaling symmetry-related structure factors $F(\mathbf{H})$ of the Penrose tiling (edge length $a_r = 4.04$ Å) in perpendicular space. Enlarged sections of positive (above) and negative structure factors (below) are shown.

$$\Gamma(\alpha) = \begin{pmatrix} 1 & 0 & 0 & 0 & 0 & 0 \\ 0 & 0 & 0 & 0 & 0 & 1 \\ 0 & 1 & 0 & 0 & 0 & 0 \\ 0 & 0 & 1 & 0 & 0 & 0 \\ 0 & 0 & 0 & 1 & 0 & 0 \\ 0 & 0 & 0 & 0 & 1 & 0 \end{pmatrix}_D, \Gamma(\beta) = \begin{pmatrix} 0 & 1 & 0 & 0 & 0 & 0 \\ 0 & 0 & 0 & 0 & 0 & 1 \\ 0 & 0 & 0 & \bar{1} & 0 & 0 \\ 0 & 0 & 0 & 0 & \bar{1} & 0 \\ 0 & 0 & 1 & 0 & 0 & 0 \\ 1 & 0 & 0 & 0 & 0 & 0 \end{pmatrix}_D,$$

$$\Gamma(\gamma) = \begin{pmatrix} \bar{1} & 0 & 0 & 0 & 0 & 0 \\ 0 & \bar{1} & 0 & 0 & 0 & 0 \\ 0 & 0 & \bar{1} & 0 & 0 & 0 \\ 0 & 0 & 0 & \bar{1} & 0 & 0 \\ 0 & 0 & 0 & 0 & \bar{1} & 0 \\ 0 & 0 & 0 & 0 & 0 & \bar{1} \end{pmatrix}_D.$$

Block-diagonalization of these reducible symmetry matrices decomposes them into non-equivalent irreducible representations. These can be assigned to the two orthogonal subspaces forming the 6D embedding space $\mathbf{V} = \mathbf{V}^{\parallel} \oplus \mathbf{V}^{\perp}$, the 3D parallel (physical) subspace $\mathbf{V}^{\parallel}$ and the perpendicular 3D subspace $\mathbf{V}^{\perp}$. Thus, using $W\Gamma W^{-1} = \Gamma^{\text{red}} = \Gamma^{\parallel} \oplus \Gamma^{\perp}$, we obtain

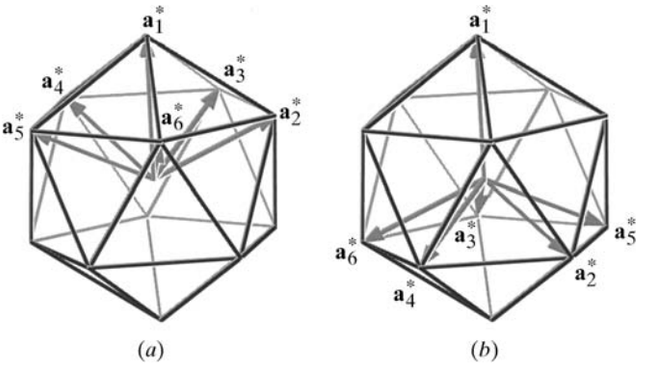

Fig. 4.6.3.28. Perspective (*a*) parallel- and (*b*) perpendicular-space views of the reciprocal basis of the 3D Penrose tiling. The six rationally independent vectors $\mathbf{a}_i^*$ point to the edges of an icosahedron.

$$\Gamma(\alpha) = \left(\begin{array}{ccc|ccc} \cos(2\pi/5) & -\sin(2\pi/5) & 0 & 0 & 0 & 0 \\ \sin(2\pi/5) & \cos(2\pi/5) & 0 & 0 & 0 & 0 \\ 0 & 0 & 1 & 0 & 0 & 0 \\ \hline 0 & 0 & 0 & \cos(4\pi/5) & -\sin(4\pi/5) & 0 \\ 0 & 0 & 0 & \sin(4\pi/5) & \cos(4\pi/5) & 0 \\ 0 & 0 & 0 & 0 & 0 & 1 \end{array}\right)_V$$
$$= \left(\begin{array}{c|c} \Gamma^{\parallel} & 0 \\ \hline 0 & \Gamma^{\perp} \end{array}\right)_V,$$

where

$$W = a^* \begin{pmatrix} 0 & sc4 & sc6 & sc8 & s & sc2 \\ 0 & ss4 & ss6 & ss8 & 0 & ss2 \\ 1 & c & c & c & c & c \\ \hline 0 & -sc8 & -sc2 & -sc6 & -s & -sc4 \\ 0 & -ss8 & -ss2 & -ss6 & 0 & -ss4 \\ 1 & -c & -c & -c & -c & -c \end{pmatrix}_V,$$

$c = \cos\theta$, $s = \sin\theta$, $scn = \sin\theta\cos(n\pi/5)$, $ssn = \sin\theta\sin(n\pi/5)$. The column vectors of the matrix W give the parallel- (above the partition line) and perpendicular-space components (below the partition line) of a reciprocal basis in $\mathbf{V}$. Thus, W can be rewritten using the physical-space reciprocal basis defined above and an arbitrary constant c,

$$W = \begin{pmatrix} \mathbf{a}_1^* & \mathbf{a}_2^* & \mathbf{a}_3^* & \mathbf{a}_4^* & \mathbf{a}_5^* & \mathbf{a}_6^* \\ c\mathbf{a}_1^* & -c\mathbf{a}_4^* & -c\mathbf{a}_6^* & -c\mathbf{a}_3^* & -c\mathbf{a}_5^* & -c\mathbf{a}_2^* \end{pmatrix}$$
$$= (\,\mathbf{d}_1^* \quad \mathbf{d}_2^* \quad \mathbf{d}_3^* \quad \mathbf{d}_4^* \quad \mathbf{d}_5^* \quad \mathbf{d}_6^*\,),$$

yielding the reciprocal basis $\mathbf{d}_i^*, i = 1, \ldots, 6$, in the 6D embedding space (*D* space)

$$\mathbf{d}_1^* = a^* \begin{pmatrix} 0 \\ 0 \\ 1 \\ 0 \\ 0 \\ c \end{pmatrix} \text{ and } \mathbf{d}_i^* = a^* \begin{pmatrix} \sin\theta\cos(2\pi i/5) \\ \sin\theta\sin(2\pi i/5) \\ \cos\theta \\ -c\sin\theta\cos(4\pi i/5) \\ -c\sin\theta\sin(4\pi i/5) \\ -c\cos\theta \end{pmatrix}, i = 2, \ldots, 6.$$

The 6×6 symmetry matrices can each be decomposed into two 3×3 matrices. The first one, $\Gamma^{\parallel}$, acts on the parallel-space component, the second one, $\Gamma^{\perp}$, on the perpendicular-space component. In the case of $\Gamma(\alpha)$, the coupling factor between a rotation in parallel and perpendicular space is 2. Thus a $2\pi/5$

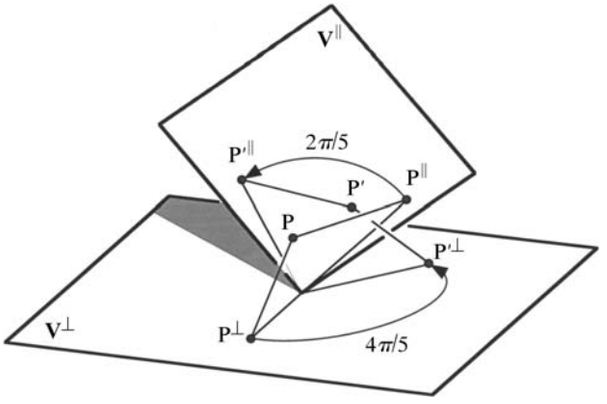

Fig. 4.6.3.29. Schematic representation of a rotation in 6D space. The point P is rotated to P′. The component rotations in parallel and perpendicular space are illustrated.

rotation in physical space is related to a $4\pi/5$ rotation in perpendicular space (Figs. 4.6.3.28 and 4.6.3.29).

With the condition $\mathbf{d}_i \cdot \mathbf{d}_j^* = \delta_{ij}$, the basis in direct 6D space is obtained:

$$\mathbf{d}_1 = \frac{1}{2a^*}\begin{pmatrix} 0 \\ 0 \\ 1 \\ 0 \\ 0 \\ 1/c \end{pmatrix} \text{ and } \mathbf{d}_i = \frac{1}{2a^*}\begin{pmatrix} \sin\theta\cos(2\pi i/5) \\ \sin\theta\sin(2\pi i/5) \\ \cos\theta \\ -(1/c)\sin\theta\cos(4\pi i/5) \\ -(1/c)\sin\theta\sin(4\pi i/5) \\ -(1/c)\cos\theta \end{pmatrix}, \quad i = 2, \ldots, 6.$$

The metric tensors G, G^* are of the type

$$\begin{pmatrix} A & B & B & B & B & B \\ B & A & B & -B & -B & B \\ B & B & A & B & -B & -B \\ B & -B & B & A & B & -B \\ B & -B & -B & B & A & B \\ B & B & -B & -B & B & A \end{pmatrix},$$

with $A = (1+c^2)a^{*2}, B = [(5)^{1/2}/5](1-c^2)a^{*2}$ for the reciprocal space and $A = (1+c^2)/[4(ca^*)^2]$ $B = [(5)^{1/2}(c^2-1)]/[20(ca^*)^2]$ for the direct space. For $c = 1$ we obtain hypercubic direct and reciprocal 6D lattices.

The lattice parameters in reciprocal and direct space are $d_i^* = a^*(2)^{1/2}$ and $d_i = 1/[(2)^{1/2}a^*]$ with $i = 1, \ldots, 6$, respectively. The volume of the 6D unit cell can be calculated from the metric tensor G. For $c = 1$ it is simply $V = [\det(G)]^{1/2} = \{1/[(2)^{1/2}a^*]\}^6$.

The best known example of a 3D quasiperiodic structure is the canonical 3D *Penrose tiling* (see Janssen, 1986). It can be constructed from two unit tiles: a prolate and an oblate rhombohedron with equal edge lengths a_r (Fig. 4.6.3.30). Each face of the rhombohedra is a rhomb with acute angles $\alpha_r = \text{arc cos}[1/(5)^{1/2}] \simeq 63.44°$. Their volumes are $V_p = (4/5)a_r^3 \sin(2\pi/5), V_o = (4/5)a_r^3 \sin(\pi/5) = V_p/\tau$, and their frequencies $\nu_p{:}\nu_o = \tau{:}1$. The resulting point density (number of vertices per unit volume) is $\rho_p = (\tau+1)/(\tau V_p + V_o) = (\tau/a_r^3)\sin(2\pi/5)$. Ten prolate and ten oblate rhombohedra can be packed to form a rhombic triacontahedron. The icosahedral symmetry of this zonohedron is broken by the many possible decompositions into the rhombohedra. Removing one zone of the triacontahedron gives a rhomb-icosahedron consisting of five prolate and five oblate rhombohedra. Again, the singular fivefold axis of the rhomb-icosahedron is broken by the decomposition into rhombohedra. Removing one zone again gives a rhombic dodecahedron consisting of two prolate and two oblate rhombohedra. Removing the last remaining zone leads finally to a single prolate rhombohedron. Using these zonohedra as elementary clusters, a matching rule can be derived for the 3D construction of the 3D Penrose tiling (Levine & Steinhardt, 1986; Socolar & Steinhardt, 1986).

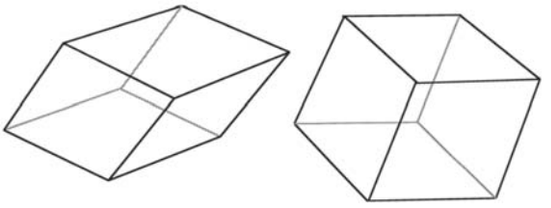

Fig. 4.6.3.30. The two unit tiles of the 3D Penrose tiling: a prolate $[\alpha_p = \text{arc cos}(5^{-1/2}) \simeq 63.44°]$ and an oblate $(\alpha_o = 180° - \alpha_p)$ rhombohedron with equal edge lengths a_r.

The 3D Penrose tiling can be embedded in the 6D space as shown above. The 6D hypercubic lattice is decorated on the lattice nodes with 3D triacontahedra obtained from the projection of a 6D unit cell upon the perpendicular space $\mathbf{V}^\perp$ (Fig. 4.6.3.31). Thus the edge length of the rhombs covering the triacontahedron is equivalent to the length $\pi^\perp(\mathbf{d}_i) = 1/2a^*$ of the perpendicular-space component of the vectors spanning the 6D hypercubic lattice $\Sigma = \{\mathbf{r} = \sum_{i=1}^6 n_i \mathbf{d}_i | n_i \in \mathbb{Z}\}$.

4.6.3.3.3.1. *Indexing*

There are several indexing schemes in use. The generic one uses a set of six rationally independent reciprocal-basis vectors pointing to the corners of an icosahedron, $\mathbf{a}_1^* = a^*(0,0,1)$, $\mathbf{a}_i^* = a^*[\sin\theta\cos(2\pi i/5), \sin\theta\sin(2\pi i/5), \cos\theta]$, $i = 2, \ldots, 6$, $\sin\theta = 2/(5)^{1/2}$, $\cos\theta = 1/(5)^{1/2}$, with $\theta \simeq 63.44°$, the angle between two neighbouring fivefold axes (setting 1) (Fig. 4.6.3.28). In this case, the physical-space basis corresponds to a simple projection of the 6D reciprocal basis $\mathbf{d}_i^*, i = 1, \ldots, 6$. Sometimes, the same set of six reciprocal-basis vectors is referred to a differently oriented Cartesian reference system (C basis, with

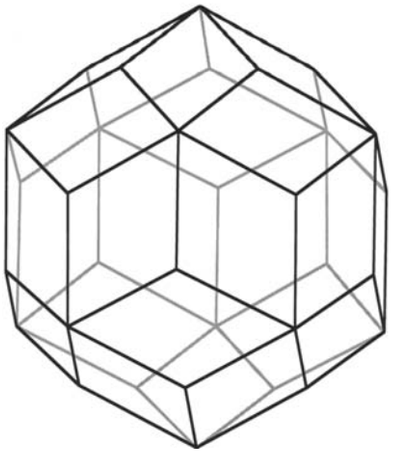

Fig. 4.6.3.31. Atomic surface of the 3D Penrose tiling in the 6D hypercubic description. The projection of the 6D hypercubic unit cell upon $\mathbf{V}^\perp$ gives a rhombic triacontahedron.

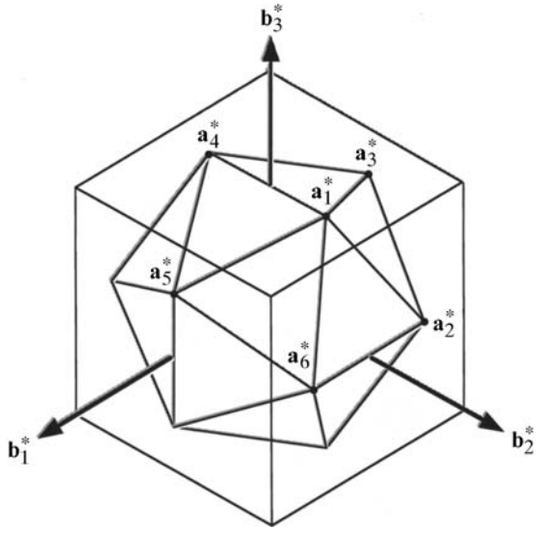

Fig. 4.6.3.32. Perspective parallel-space view of the two alternative reciprocal bases of the 3D Penrose tiling: the cubic and the icosahedral setting, represented by the bases $\mathbf{b}_i^*, i = 1, \ldots, 3$, and $\mathbf{a}_i^*, i = 1, \ldots, 6$, respectively.

basis vectors $\mathbf{e}_i$ along the twofold axes) (Bancel *et al.*, 1985). The reciprocal basis is

$$\begin{pmatrix} \mathbf{a}_1^* \\ \mathbf{a}_2^* \\ \mathbf{a}_3^* \\ \mathbf{a}_4^* \\ \mathbf{a}_5^* \\ \mathbf{a}_6^* \end{pmatrix} = \frac{a^*}{(1+\tau^2)^{1/2}} \begin{pmatrix} 0 & 1 & \tau \\ -1 & \tau & 0 \\ -\tau & 0 & 1 \\ 0 & -1 & \tau \\ \tau & 0 & 1 \\ 1 & \tau & 0 \end{pmatrix}_C \begin{pmatrix} \mathbf{e}_1^C \\ \mathbf{e}_2^C \\ \mathbf{e}_3^C \end{pmatrix}.$$

An alternate way of indexing is based on a 3D set of cubic reciprocal-basis vectors $\mathbf{b}_i^*, i = 1, \ldots, 3$ (setting 2) (Fig. 4.6.3.32):

$$\begin{pmatrix} \mathbf{b}_1^* \\ \mathbf{b}_2^* \\ \mathbf{b}_3^* \end{pmatrix} = \frac{1}{2} \begin{pmatrix} 0 & \bar{1} & 0 & 0 & 0 & 1 \\ 1 & 0 & 0 & \bar{1} & 0 & 0 \\ 0 & 0 & 1 & 0 & 1 & 0 \end{pmatrix}_D \begin{pmatrix} \mathbf{a}_1^* \\ \mathbf{a}_2^* \\ \mathbf{a}_3^* \\ \mathbf{a}_4^* \\ \mathbf{a}_5^* \\ \mathbf{a}_6^* \end{pmatrix}$$

$$= \frac{a^*}{(1+\tau^2)^{1/2}} \begin{pmatrix} \mathbf{e}_1^C \\ \mathbf{e}_2^C \\ \mathbf{e}_3^C \end{pmatrix}.$$

The Cartesian C basis is related to the V basis by a $\theta/2$ rotation around $[100]_C$, yielding $[001]_V$, followed by a $\pi/10$ rotation around $[001]_C$:

$$\begin{pmatrix} \mathbf{e}_1^C \\ \mathbf{e}_2^C \\ \mathbf{e}_3^C \end{pmatrix} = \begin{pmatrix} \cos(\pi/10) & \sin(\pi/10) & 0 \\ -\cos(\theta/2)\sin(\pi/10) & \cos(\theta/2)\cos(\pi/10) & \sin(\theta/2) \\ \sin(\theta/2)\sin(\pi/10) & -\sin(\theta/2)\cos(\pi/10) & \cos(\theta/2) \end{pmatrix}_V \begin{pmatrix} \mathbf{e}_1^V \\ \mathbf{e}_2^V \\ \mathbf{e}_3^V \end{pmatrix}.$$

Thus, indexing the diffraction pattern of an icosahedral phase with integer indices, one obtains for setting 1 $\mathbf{H} = \sum_{i=1}^{6} h_i \mathbf{a}_i^*, h_i \in \mathbb{Z}$. These indices $(h_1\ h_2\ h_3\ h_4\ h_5\ h_6)$ transform into the second setting to $(h/h'\ k/k'\ l/l')$ with the fractional cubic indices $h_1^c = h + h'\tau, h_2^c = k + k'\tau, h_3^c = l + l'\tau$. The transformation matrix is

$$\begin{pmatrix} h \\ h' \\ k \\ k' \\ l \\ l' \end{pmatrix}_C = \begin{pmatrix} 0 & \bar{1} & 0 & 0 & 0 & 1 \\ 0 & 0 & \bar{1} & 0 & 1 & 0 \\ 1 & 0 & 0 & \bar{1} & 0 & 0 \\ 0 & 1 & 0 & 0 & 0 & 1 \\ 0 & 0 & 1 & 0 & 1 & 0 \\ 1 & 0 & 0 & 1 & 0 & 0 \end{pmatrix} \begin{pmatrix} h_1 \\ h_2 \\ h_3 \\ h_4 \\ h_5 \\ h_6 \end{pmatrix}_D = \begin{pmatrix} h_6 - h_2 \\ h_5 - h_3 \\ h_1 - h_4 \\ h_6 + h_2 \\ h_5 + h_3 \\ h_1 + h_4 \end{pmatrix}_D.$$

4.6.3.3.3.2. *Diffraction symmetry*

The diffraction symmetry of icosahedral phases can be described by the Laue group $K = m\bar{3}\bar{5}$. The set of all vectors $\mathbf{H}$ forms a Fourier module $M^* = \{\mathbf{H}^{\parallel} = \sum_{i=1}^{6} h_i \mathbf{a}_i^* | h_i \in \mathbb{Z}\}$ of rank 6 in physical space. Consequently, it can be considered as a projection from a 6D reciprocal lattice, $M^* = \pi^{\parallel}(\Sigma^*)$. The parallel and perpendicular reciprocal-space sections of the 3D Penrose tiling decorated with equal point scatterers on its vertices are shown in Figs. 4.6.3.33 and 4.6.3.34. The diffraction pattern in perpendicular space is the Fourier transform of the triacontahedron. All Bragg reflections within $10^{-4}|F(\mathbf{0})|^2 < |F(\mathbf{H})|^2 < |F(\mathbf{0})|^2$ are depicted. Without intensity-truncation limit, the diffraction pattern would be densely filled with discrete Bragg reflections.

The 6D icosahedral space groups that are relevant to the description of icosahedral phases (six symmorphous and five non-symmorphous groups) are listed in Table 4.6.3.2. These space groups are a subset of all 6D icosahedral space groups fulfilling the condition that the 6D point groups they are associated with are isomorphous to the 3D point groups $\frac{2}{m}\bar{3}\bar{5}$ and 235 describing the diffraction symmetry. From 826 6D (analogues to) Bravais groups (Levitov & Rhyner, 1988), only three fulfil the condition that the projection of the 6D hypercubic lattice upon the 3D physical space is compatible with the icosahedral point groups $\frac{2}{m}\bar{3}\bar{5}$, 235: the primitive hypercubic Bravais lattice P, the body-centred Bravais lattice I with translation 1/2(111111), and the face-centred Bravais lattice F with translations $1/2(110000) + 14$ further cyclic permutations. Hence, the I lattice is twofold primitive (*i.e.* it contains two vertices per unit cell) and the F lattice is 16-fold primitive. The orientation of the symmetry elements in the 6D space is defined by the isomorphism of the 3D and 6D point groups. The action of the fivefold rotation, however, is different in the subspaces $\mathbf{V}^{\parallel}$ and $\mathbf{V}^{\perp}$: a rotation of $2\pi/5$ in $\mathbf{V}^{\parallel}$ is correlated with a rotation of $4\pi/5$ in $\mathbf{V}^{\perp}$. The reflection and inversion operations are equivalent in both subspaces.

4.6.3.3.3.3. *Structure factor*

The structure factor of the icosahedral phase corresponds to the Fourier transform of the 6D unit cell,

$$F(\mathbf{H}) = \sum_{k=1}^{N} f_k(\mathbf{H}^{\parallel}) T_k(\mathbf{H}^{\parallel}, \mathbf{H}^{\perp}) g_k(\mathbf{H}^{\perp}) \exp(2\pi i \mathbf{H} \cdot \mathbf{r}_k),$$

with 6D diffraction vectors $\mathbf{H} = \sum_{i=1}^{6} h_i \mathbf{d}_i^*$, parallel-space atomic scattering factor $f_k(H^{\parallel})$, temperature factor $T_k(\mathbf{H}^{\parallel}, \mathbf{H}^{\perp})$, and perpendicular-space geometric form factor $g_k(\mathbf{H}^{\perp})$. $T_k(\mathbf{H}^{\parallel}, \mathbf{0})$ is equivalent to the conventional Debye–Waller factor and $T_k(\mathbf{0}, \mathbf{H}^{\perp})$ describes random fluctuations in perpendicular space. These fluctuations cause characteristic jumps of vertices (*phason flips*) in the physical space. Even random phason flips map the vertices onto positions that can still be described by physical-space vectors of the type $\mathbf{r} = \sum_{i=1}^{6} n_i \mathbf{a}_i$. Consequently, the set $M = \{\mathbf{r} = \sum_{i=1}^{6} n_i \mathbf{a}_i | n_i \in \mathbb{Z}\}$ of all possible vectors forms a $\mathbb{Z}$ module. The shape of the atomic surfaces corresponds to a selection rule for the positions actually occupied. The geometric form factor $g_k(\mathbf{H}^{\perp})$ is equivalent to the Fourier transform of the *atomic surface*, *i.e.* the 3D perpendicular-space component of the 6D *hyperatoms*.

For the example of the canonical 3D Penrose tiling, $g_k(\mathbf{H}^{\perp})$ corresponds to the Fourier transform of a triacontahedron:

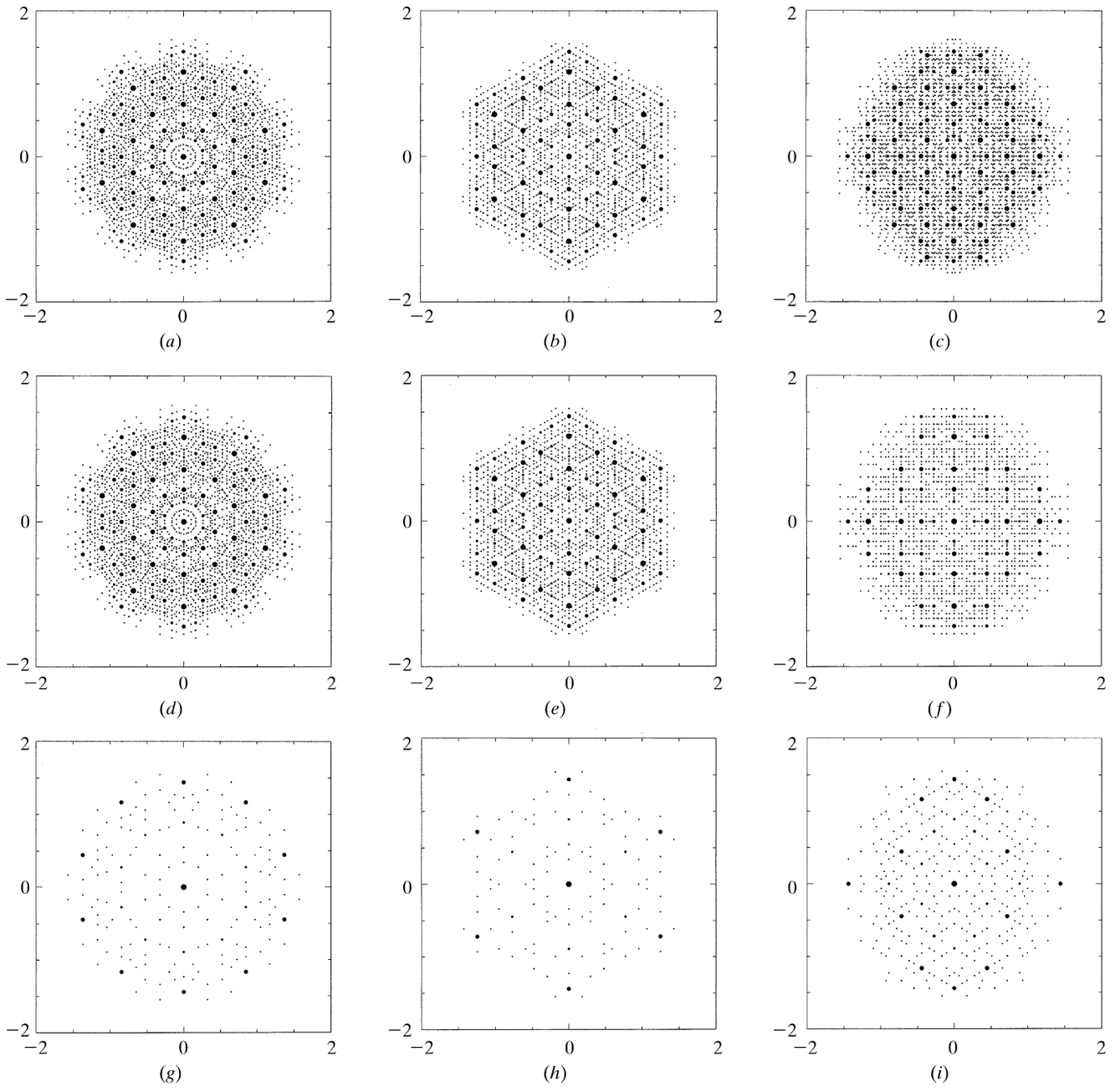

Fig. 4.6.3.33. Physical-space diffraction patterns of the 3D Penrose tiling decorated with point atoms (edge lengths of the Penrose unit rhombohedra $a_r = 5.0$ Å). Sections with five-, three- and twofold symmetry are shown for the primitive 6D analogue of Bravais type P in (a, b, c), the body-centred 6D analogue to Bravais type I in (d, e, f) and the face-centred 6D analogue to Bravais type F in (g, h, i). All reflections are shown within $10^{-4}|F(\mathbf{0})|^2 < |F(\mathbf{H})|^2 < |F(\mathbf{0})|^2$ and $-6 \le h_i \le 6, i = 1, \ldots, 6$.

$$g_k(\mathbf{H}^\perp) = (1/A_{\rm UC}^\perp) \int_{A_k} \exp(2\pi i \mathbf{H}^\perp \cdot \mathbf{r})\ \mathrm{d}\mathbf{r},$$

where $A_{\rm UC}^\perp$ is the volume of the 6D unit cell projected upon $\mathbf{V}^\perp$ and A_k is the volume of the triacontahedron. $A_{\rm UC}^\perp$ and A_k are equal in the present case and amount to the volumes of ten prolate and ten oblate rhombohedra: $A_{\rm UC}^\perp = 8a_r^3[\sin(2\pi/5) + \sin(\pi/5)]$. Evaluating the integral by decomposing the triacontahedron into trigonal pyramids, each one directed from the centre of the triacontahedron to three of its corners given by the vectors $\mathbf{e}_i, i = 1, \ldots, 3$, one obtains

$$g(\mathbf{H}^\perp) = (1/A_{\rm UC}^\perp) \sum_R g_k(R^T \mathbf{H}^\perp),$$

with $k = 1, \ldots, 60$ running over all site-symmetry operations R of the icosahedral group,

$$\begin{aligned} g_k(\mathbf{H}^\perp) = -iV_r[&A_2A_3A_4 \exp(iA_1) + A_1A_3A_5 \exp(iA_2) \\ &+ A_1A_2A_6 \exp(iA_3) + A_4A_5A_6] \\ &\times (A_1A_2A_3A_4A_5A_6)^{-1}, \end{aligned}$$

$A_j = 2\pi \mathbf{H}^\perp \cdot \mathbf{e}_j$, $j = 1, \ldots, 3$, $A_4 = A_2 - A_3$, $A_5 = A_3 - A_1$, $A_6 = A_1 - A_2$ and $V_r = \mathbf{e}_1 \cdot (\mathbf{e}_2 \times \mathbf{e}_3)$ the volume of the parallelepiped defined by the vectors $\mathbf{e}_i, i = 1, \ldots, 3$ (Yamamoto, 1992*b*).

4.6.3.3.3.4. *Intensity statistics*

The radial structure-factor distributions of the 3D Penrose tiling decorated with point scatterers are plotted in Fig. 4.6.3.35 as a function of parallel and perpendicular space. The distribution of $|F(\mathbf{H})|$ as a function of their frequencies clearly resembles a centric

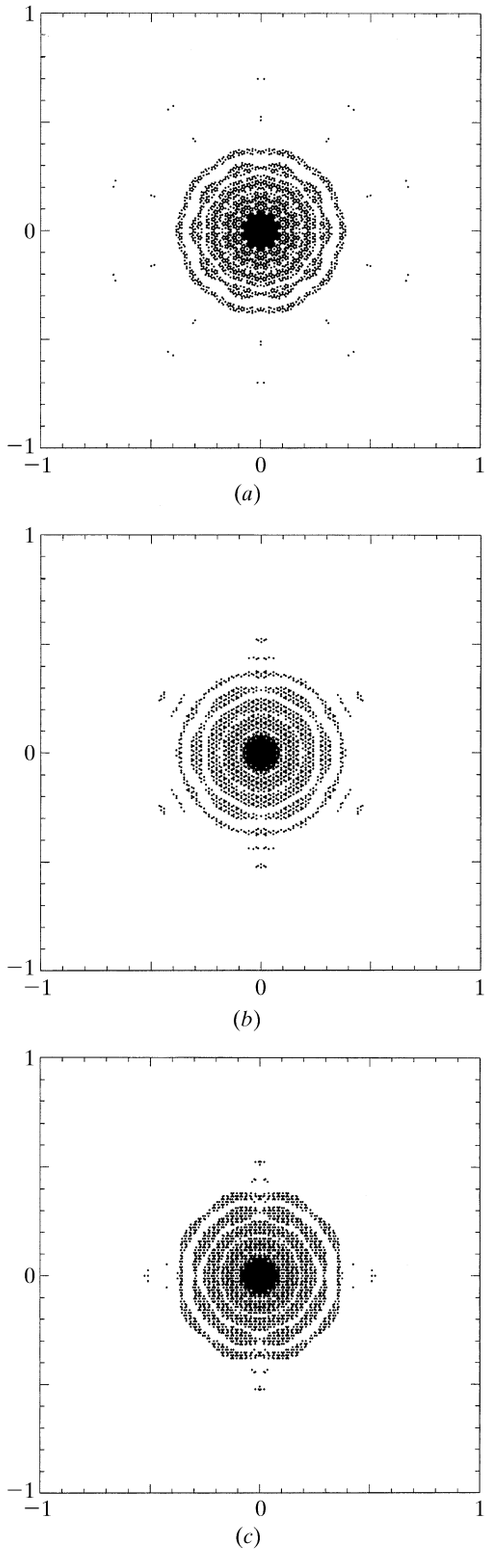

Fig. 4.6.3.34. Perpendicular-space diffraction patterns of the 3D Penrose tiling decorated with point atoms (edge lengths of the Penrose unit rhombohedra $a_r = 5.0$ Å). Sections with (*a*) five-, (*b*) three- and (*c*) twofold symmetry are shown for the primitive 6D analogue of Bravais type $P_{\bar{3}\bar{5}}$. All reflections are shown within $10^{-4}|F(\mathbf{0})|^2 < |F(\mathbf{H})|^2 < |F(\mathbf{0})|^2$ and $-6 \le h_i \le 6, i = 1, \ldots, 6$.

Table 4.6.3.2. *3D point groups of order k describing the diffraction symmetry and corresponding 6D decagonal space groups with reflection conditions (see Levitov & Rhyner, 1988; Rokhsar et al., 1988)*

3D point group	k	5D space group	Reflection condition
$\frac{2}{m}\bar{3}\bar{5}$	120	$P\frac{2}{m}\bar{3}\bar{5}$	No condition
		$P\frac{2}{n}\bar{3}\bar{5}$	$h_1h_2\overline{h_1h_2}h_5h_6 : h_5 - h_6 = 2n$
		$I\frac{2}{m}\bar{3}\bar{5}$	$h_1h_2h_3h_4h_5h_6 : \sum_{i=1}^{6} h_i = 2n$
		$F\frac{2}{m}\bar{3}\bar{5}$	$h_1h_2h_3h_4h_5h_6 : \sum_{i\neq j=1}^{6} h_i + h_j = 2n$
		$F\frac{2}{n}\bar{3}\bar{5}$	$h_1h_2h_3h_4h_5h_6 : \sum_{i\neq j=1}^{6} h_i + h_j = 2n$ $h_1h_2\overline{h_1h_2}h_5h_6 : h_5 - h_6 = 4n$
235	60	$P235$	No condition
		$P235_1$	$h_1h_2h_2h_2h_2h_2 : h_1 = 5n$
		$I235$	$h_1h_2h_3h_4h_5h_6 : \sum_{i=1}^{6} h_i = 2n$
		$I235_1$	$h_1h_2h_3h_4h_5h_6 : \sum_{i=1}^{6} h_i = 2n$ $h_1h_2h_2h_2h_2h_2 : h_1 + 5h_2 = 10n$
		$F235$	$h_1h_2h_3h_4h_5h_6 : \sum_{i\neq j=1}^{6} h_i + h_j = 2n$
		$F235_1$	$h_1h_2h_3h_4h_5h_6 : \sum_{i\neq j=1}^{6} h_i + h_j = 2n$ $h_1h_2h_2h_2h_2h_2 : h_1 + 5h_2 = 10n$

distribution, as can be expected from the centrosymmetric unit cell. The shape of the distribution function depends on the radius of the limiting sphere in reciprocal space. The number of weak reflections increases as the power 6, that of strong reflections only as the power 3 (strong reflections always have small $\mathbf{H}^{\perp}$ components).

The weighted reciprocal space of the 3D Penrose tiling contains an infinite number of Bragg reflections within a limited region of the physical space. Contrary to the diffraction pattern of a periodic structure consisting of point atoms on the lattice nodes, the Bragg reflections show intensities depending on the perpendicular-space components of their diffraction vectors.

4.6.3.3.3.5. *Relationships between structure factors at symmetry-related points of the Fourier image*

The weighted 3D reciprocal space $M^* = \{\mathbf{H}^{\parallel} = \sum_{i=1}^{6} h_i \mathbf{a}_i^* | h_i \in \mathbb{Z}\}$ exhibits the icosahedral point symmetry $K = m\bar{3}\bar{5}$. It is invariant under the action of the scaling matrix S^3:

$$S = \frac{1}{2}\begin{pmatrix} 1 & 1 & 1 & 1 & 1 & 1 \\ 1 & 1 & 1 & -1 & -1 & 1 \\ 1 & 1 & 1 & 1 & -1 & -1 \\ 1 & -1 & 1 & 1 & 1 & -1 \\ 1 & -1 & -1 & 1 & 1 & 1 \\ 1 & 1 & -1 & -1 & 1 & 1 \end{pmatrix}_D, S^3 = \begin{pmatrix} 2 & 1 & 1 & 1 & 1 & 1 \\ 1 & 2 & 1 & -1 & -1 & 1 \\ 1 & 1 & 2 & 1 & -1 & -1 \\ 1 & -1 & 1 & 2 & 1 & -1 \\ 1 & -1 & -1 & 1 & 2 & 1 \\ 1 & 1 & -1 & -1 & 1 & 2 \end{pmatrix}_D,$$

$$\begin{pmatrix} 2 & 1 & 1 & 1 & 1 & 1 \\ 1 & 2 & 1 & -1 & -1 & 1 \\ 1 & 1 & 2 & 1 & -1 & -1 \\ 1 & -1 & 1 & 2 & 1 & -1 \\ 1 & -1 & -1 & 1 & 2 & 1 \\ 1 & 1 & -1 & -1 & 1 & 2 \end{pmatrix}_D \begin{pmatrix} \mathbf{a}_1^* \\ \mathbf{a}_2^* \\ \mathbf{a}_3^* \\ \mathbf{a}_4^* \\ \mathbf{a}_5^* \\ \mathbf{a}_6^* \end{pmatrix} = \tau^3 \begin{pmatrix} \mathbf{a}_1^* \\ \mathbf{a}_2^* \\ \mathbf{a}_3^* \\ \mathbf{a}_4^* \\ \mathbf{a}_5^* \\ \mathbf{a}_6^* \end{pmatrix}.$$

The scaling transformation $\left(S^{-3}\right)^T$ leaves a primitive 6D reciprocal lattice invariant as can easily be seen from its application on the indices:

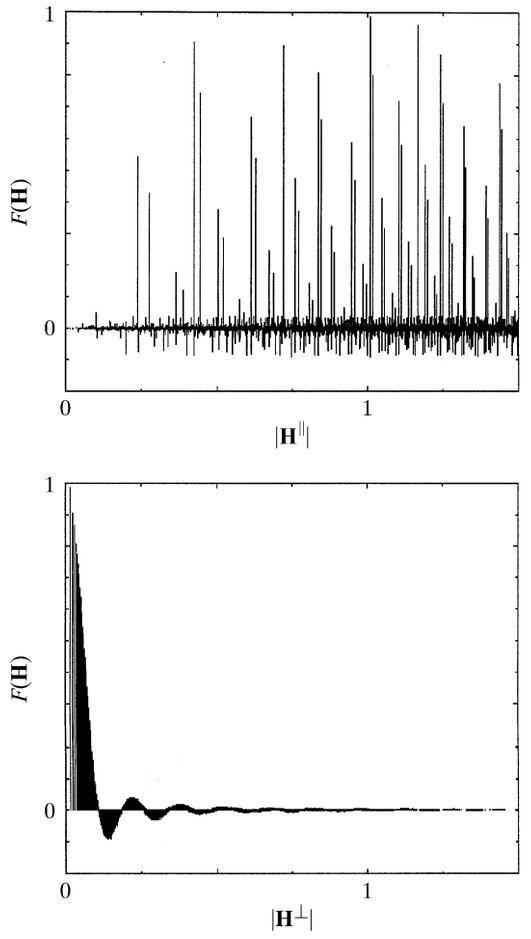

Fig. 4.6.3.35. Radial distribution function of the structure factors $F(\mathbf{H})$ of the 3D Penrose tiling (edge lengths of the Penrose unit rhombohedra $a_r = 5.0$ Å) decorated with point atoms as a function of $|\mathbf{H}^{\parallel}|$ (above) and $|\mathbf{H}^{\perp}|$ (below). All reflections are shown within $10^{-6}|F(\mathbf{0})|^2 < |F(\mathbf{H})|^2 < |F(\mathbf{0})|^2$ and $-6 \le h_i \le 6, i = 1, \ldots, 6$.

$$\begin{pmatrix} h_1' \\ h_2' \\ h_3' \\ h_4' \\ h_5' \\ h_6' \end{pmatrix} = \begin{pmatrix} -2 & 1 & 1 & 1 & 1 & 1 \\ 1 & -2 & 1 & -1 & -1 & 1 \\ 1 & 1 & -2 & 1 & -1 & -1 \\ 1 & -1 & 1 & -2 & 1 & -1 \\ 1 & -1 & -1 & 1 & -2 & 1 \\ 1 & 1 & -1 & -1 & 1 & -2 \end{pmatrix}_D \begin{pmatrix} h_1 \\ h_2 \\ h_3 \\ h_4 \\ h_5 \\ h_6 \end{pmatrix}.$$

The matrix $(S^{-1})^T$ leaves $M^* = \{\mathbf{H}^{\parallel} = \sum_{i=1}^{6} h_i \mathbf{a}_i^* | h_i \in \mathbb{Z}\}$ invariant,

$$\begin{pmatrix} h_1' \\ h_2' \\ h_3' \\ h_4' \\ h_5' \\ h_6' \end{pmatrix} = \frac{1}{2} \begin{pmatrix} -1 & 1 & 1 & 1 & 1 & 1 \\ 1 & -1 & 1 & -1 & -1 & 1 \\ 1 & 1 & -1 & 1 & -1 & -1 \\ 1 & -1 & 1 & -1 & 1 & -1 \\ 1 & -1 & -1 & 1 & -1 & 1 \\ 1 & 1 & -1 & -1 & 1 & -1 \end{pmatrix}_D \begin{pmatrix} h_1 \\ h_2 \\ h_3 \\ h_4 \\ h_5 \\ h_6 \end{pmatrix},$$

for any $\mathbf{H} = \sum_{i=1}^{6} h_i \mathbf{d}_i^*$ with h_i all even or all odd, corresponding to a 6D face-centred hypercubic lattice. In a second case the sum $\sum_{i=1}^{6} h_i$ is even, corresponding to a 6D body-centred hypercubic lattice. Block-diagonalization of the matrix S decomposes it into two irreducible representations. With $WSW^{-1} = S_V = S_V^{\parallel} \oplus S_V^{\perp}$ we obtain

$$S_V = \left(\begin{array}{ccc|ccc} \tau & 0 & 0 & 0 & 0 & 0 \\ 0 & \tau & 0 & 0 & 0 & 0 \\ 0 & 0 & \tau & 0 & 0 & 0 \\ \hline 0 & 0 & 0 & -1/\tau & 0 & 0 \\ 0 & 0 & 0 & 0 & -1/\tau & 0 \\ 0 & 0 & 0 & 0 & 0 & -1/\tau \end{array}\right)_V = \left(\begin{array}{c|c} S^{\parallel} & 0 \\ \hline 0 & S^{\perp} \end{array}\right)_V,$$

the scaling properties in the two 3D subspaces: scaling by a factor τ in parallel space corresponds to a scaling by a factor $(-\tau)^{-1}$ in perpendicular space. For the intensities of the scaled reflections analogous relationships are valid, as discussed for decagonal phases (Figs. 4.6.3.36 and 4.6.3.37, Section 4.6.3.3.2.5).

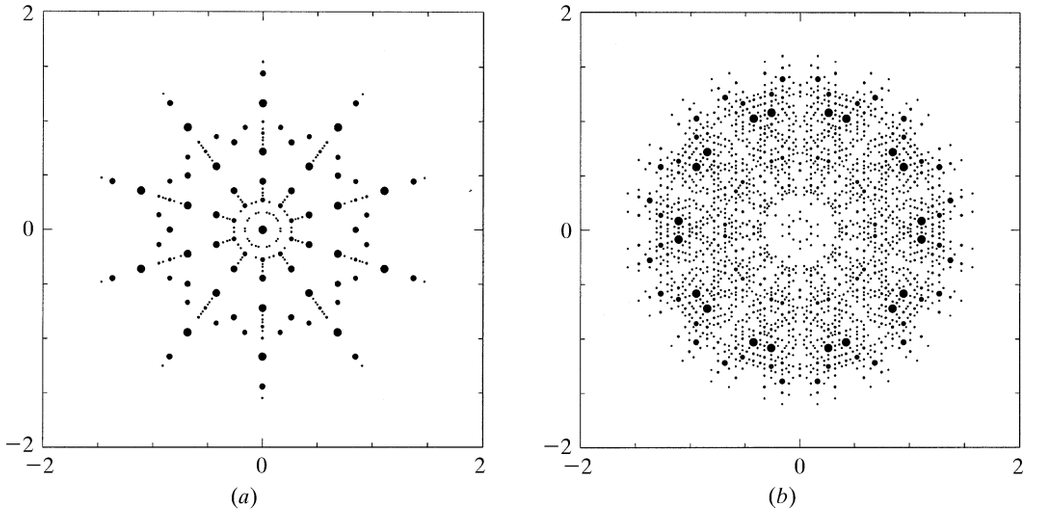

Fig. 4.6.3.36. Parallel-space distribution of (*a*) positive and (*b*) negative structure factors of the 3D Penrose tiling of the 6D *P* lattice type decorated with point atoms (edge lengths of the Penrose unit rhombohedra $a_r = 5.0$ Å). The magnitudes of the structure factors are indicated by the diameters of the filled circles. All reflections are shown within $10^{-4}|F(\mathbf{0})|^2 < |F(\mathbf{H})|^2 < |F(\mathbf{0})|^2$ and $-6 \le h_i \le 6, i = 1, \ldots, 6$.

references